Hypercementosis Associated with *ENPP1* Mutations and GACI

V. Thumbigere-Math, A. Alqadi, N.I. Chalmers, M.B. Chavez, E.Y. Chu, M.T. Collins, C.R. Ferreira, K. FitzGerald, R.I. Gafni, W.A. Gahl, K.S. Hsu, M.S. Ramnitz, M.J. Somerman, S.G. Ziegler, and B.L. Foster

APPENDIX

MATERIALS AND METHODS

Genetic Sequencing

As part of GACI diagnosis, all subjects had undergone genetic sequencing to identify mutations in *ENPP1* prior to enrollment in this study. Therefore, detailed sequencing methods common to all subjects were not available. *ENPP1* mutations subject 2 (Li et al. 2012), subject 4 (Rutsch et al. 2008), and subject 5 (Ferreira et al. 2016) have been reported elsewhere. All but one of the *ENPP1* mutations reported in this paper fall within the catalytic domain of ENPP1, necessary for enzymatic function of the enzyme. Previous studies using bioinformatics approaches and *in vitro* functional analyses indicate that nonsense mutations within the catalytic domain significantly affect enzyme function and elaboration of PP_i. The P305T (cases 1 and 4), H500P (case 1), Y513C (case 2), P250L (case 4), and Y471C (case 5) mutations have been previously analyzed using X-ray crystallography of native ENPP1 and computational mutagenesis of these missense mutations, and all of these mutations were found to affect protein stability, likely negatively affecting enzyme function (Jansen et al. 2012). In a study using mutated ENPP1 transfected into HEK293 or COS7 cells, P305T, Y513C, Y471C, and four more mutations in the catalytic domain all significantly decreased (by 50% or more) or completely ablated enzyme

activity, with expected decreased PP_i generation in all situations (Stella et al. 2016). Mutations in the nuclease-like domain, like G805V harbored by subject 3, also negatively affected ENPP1 enzyme activity, though more variably and sometimes less dramatically than effects from catalytic domain defects.

Inorganic Pyrophosphate (PP_i) Analysis

To determine PP_i concentrations in GACI subjects and controls, 30 µL of human plasma diluted in Ultra-pure water was reacted with 10 µL of a mixture containing 32 mU ATP sulfurylase (Sigma Aldrich, St. Louis, MO, USA), 64 µmol/L APS (Santa Cruz Biotechnology, Santa Cruz, CA, USA), 80 µmol/L $MgCl_2$, and 40 mmol/L HEPES (pH 7.40) at 37°C for 30 minutes, after which the ATP sulfurylase was inactivated by incubation of the mixture at 90°C for 10 minutes (Jansen et al. 2014). 40 µL of the resulting solution was reacted with 20 µL of BacTiterGlo (Promega, Madison, WI, USA), an ATP-monitoring reagent, and then luminescence was determined using a microplate reader (SpectraMax M5 Microplate Reader, Molecular Devices, Sunnyvale, CA, USA). PP_i standard curves were prepared to exclude matrix effects. To account for background signal caused by plasma, a second experiment was performed to assay a second aliquot of each human plasma sample after treatment with 2U/mL inorganic pyrophosphatase (Thermo Fisher Scientific, Waltham, MA, USA). A one-hour incubation in pyrophosphatase, which resulted in complete hydrolysis of plasma PP_i, was performed before repeating the assay and then subtracting those results from those of the untreated samples (Lomashvili et al. 2005).

Fibroblast Growth Factor 23 (FGF23) Analysis

Blood FGF23 was analyzed as described previously (Ramnitz et al. 2016). Briefly, intact FGF23 protein (iFGF23) was measured by ELISA (Kainos Laboratories, Tokyo, Japan; or Immunotopics International, San Clemente, CA, USA). An ELISA (Immunotopics International) designed for C-terminal FGF23 (cFGF23) detected both intact and C-terminal fragments of the protein.

Cell culture

Primary dermal fibroblasts were cultured from a 3 mm forearm punch-biopsy specimen of skin and grown in Dulbecco's modified Eagle medium (DMEM; Gibco, Gaithersburg, MD, USA) containing 10% fetal bovine serum (Lot 15C177; Sigma-Aldrich, St. Louis, MO, USA), 1 mM L-glutamine (Life Technologies, Carlsbad, CA, USA), and 1% penicillin-streptomycin (Gibco), as previously described (Normand and Karasek 1995). Cells were fed twice a week and split 1:2 at confluence.

Ectonucleotide pyrophosphatase phosphodiesterase 1 (ENPP1) enzyme activity assay

Cells were seeded in 6-well plates and grown for five days until confluence. To measure ENPP1 enzyme activity, cells were lysed in 100 mM Tris-HCl (pH 9.0), 500 mM NaCl, 5 mM MgCl2, and 0.05% Triton X-100 and scraped into microcentrifuge tubes and kept on ice. Cell suspensions were spun at 12,000 g for 5 minutes. A 50 µl aliquot of the supernatant was added to a clear-bottom 96-well plate and the reaction with initiated upon adding 50 µl of 1mM para-nitrophenol-thymidine monophosphate (pNP-TMP; Sigma-Aldrich), and allowed to proceed for 20 min. The ENPP1 assay relied on the production of p-nitrophenol (pNP) to quantify enzymatic activity, as determined by absorption at 405 nm over time (measured in minutes) and

normalized to micrograms of protein (as quantified by a bicinchoninic acid assay; Pierce, Waltham, MA, USA).

Microcomputed Tomography (Micro-CT)

Extracted and exfoliated primary teeth (6 teeth from 4 healthy controls and 10 teeth from 3 GACI subjects) were scanned in a μCT 50 (Scanco Medical, Bassersdorf, Switzerland) at 70 kVp, 76 μA, 0.5 Al filter, 900 ms integration time, and 10 μm voxel dimension. DICOM files were created and exported from scan data. Reconstructed images were loaded and analyzed in AnalyzePro 1.0 (AnalyzeDirect, Overland Park, KS). Images were oriented anatomically using the midsagittal slice, where the mesial and distal cementum-enamel junctions (CEJs) were used to identify an axis that was made perpendicular to the length of the root. Oriented scans were calibrated to a standard curve of five known hydroxyapatite (HA) densities (mg/cm^3 HA). Dentin was segmented at 650-1600 mg/cm^3 HA, and enamel was segmented above 1600 mg/cm^3 HA. For segmentation of acellular cementum, a median filter with a kernel size of 11 was applied. Acellular cementum was then segmented between 250-1050 mg/cm^3 HA with manual corrections to exclude softer dentin that was highlighted adjacent to the pulp. The cementum segmentation map was then loaded back onto the original calibrated image and used as a mask to highlight any cementum under this mask with a density over 650 mg/cm^3 HA. Quantitative analysis was then performed on the original calibrated image. Average density was determined from these volumes. Thickness was determined using cortical thickness algorithms from the most apical 50 slices that formed a hollow cylinder of acellular cementum;

if it was not possible to define 50 slices due to root resorption, then 10 random linear measurements were averaged in the same anatomical area.

First mandibular mouse molars (n=5 WT controls and n=4 *Enpp1*$^{asj/asj}$ mice at 12 wks) were scanned in a μCT 50 (Scanco Medical, Bassersdorf, Switzerland) at 70 kVp, 76 μA, 0.5 Al filter, 1200 ms integration time, and 2 μm voxel dimension. As described above, DICOM files were created, reconstructed images were loaded in AnalyzePro 1.0, and scans were calibrated to a standard curve (mg/cm³ HA). The first molar was reoriented using anatomical landmarks. In the coronal/frontal plane, the length of the mesial root was made perpendicular to the transverse plane. In the transverse plane, the mesial and distal root pulps were made perpendicular to the frontal plane. Finally, the midsagittal slice was used to orient the plane of occlusion by defining the line connecting the mesial and distal CEJs and making this line perpendicular to the transverse plane (i.e., horizontal). The oriented molar tooth is shown in Appendix Figure 1. Segmentation of enamel, dentin, and cementum was performed as described above for human teeth. After these tissues were segmented and labeled, regions of interest (ROI) were defined for purposes of analysis. Enamel thickness was determined by measuring 100 μm (50 slices) of enamel located 100 μm coronal to the CEJ (Appendix Figure 1; pink region). Crown dentin thickness was determined by measuring 100 μm (50 slices) of dentin directly coronal to the CEJ (Appendix Figure 1; green region). Root dentin thickness (of the mesial root) was determined by measuring 100 μm (50 slices) of dentin located 1/3 of the distance from CEJ to root apex (Appendix Figure 1; light blue region). Cementum was subdivided into acellular (cervical 2/3 of root length) and cellular (apical 1/3 of root length)

components (yellow and dark blue, respectively, in Appendix Figure 1), determined separately for mesial and distal roots. Acellular cementum thickness was determined by measuring 100 µm (50 slices) of cementum located 1/3 of the distance from CEJ to root apex (Appendix Figure 1; purple region). Cellular cementum thickness was determined by measuring 100 µm (50 slices) of cementum apical to the termination of root dentin (Appendix Figure 1; orange region).

Statistical analysis

Quantitative results are shown as individual measurements with mean ± standard deviation (SD) in the graphs presented. For both human and mouse data generated from micro-CT analysis, data sets were tested for normal (Gaussian) distribution by the Shapiro-Wilk test and/or visual inspection of data for skewing in cases where sample sizes were deemed insufficient for normality testing. Normal distribution of data was assumed based on testing and inspection, continuous nature of variables analyzed, and collective previous and ongoing studies on dental tissues measurements indicating normal distributions of these populations. Data were analyzed by two-tail Student's (independent samples) *t*-test, with Benjamini-Hochberg false discovery rate correction for Q = 0.05 (Benjamini and Hochberg 1995; Glickman et al. 2014). Statistical analyses were computed using GraphPad Prism 7.02 for Windows (GraphPad Software, La Jolla, CA, USA).

RESULTS

Case 1 Medical History

A 6.7-year-old Caucasian girl (subject 1) with GACI underwent dental evaluation at the NIH Clinical Center (Figure 1A-F). She was born to a 42-year-old mother at 39-weeks of gestation via Caesarean section with Apgar score of 9 at one minute and five minutes. She is the youngest of four children born to healthy non-consanguineous parents. Her older sister aged 17-years-old and older brother aged 16-years-old were reported to be healthy. Her parents reported no family history of coronary artery disease except for a previous infant son who passed away at the age of 16 weeks due to heart failure secondary to GACI. Genetic testing identified biallelic mutations in *ENPP1* (NM_006208.2:c.913C>A/p.P305T in exon 8 from the father, and c.1499A>C/p.H500P in exon 15 from the mother). The same mutations had been identified in the deceased sibling (Rutsch et al. 2008). Homozygous p.P305T mutations have been reported in at least 6 other individuals in the literature, all of whom died in infancy (Ruf et al. 2005; Rutsch et al. 2008; Stella et al. 2016).

Prenatal echocardiogram performed at 24 weeks-of-gestation for subject 1 revealed no abnormalities. At birth, she had a blood pressure of 102/58 mmHg (mean arterial blood pressure of 73 mmHg) and her cardiac troponin level was elevated (0.39 μg/L; normal range: 0.0-0.1 μg/L). Echocardiogram performed on day 1 of life showed abnormal echo-bright structures in the ascending and descending aorta, as well as pulmonary arteries. An abdominal ultrasound done on day 2 of life showed increased echodensity within the walls of the abdominal aorta, superior mesenteric artery, celiac artery, splenic artery, and right renal artery. On the same day, ultrasound examination of the head showed markedly echogenic thalamostriate and lenticulostriate vessels bilaterally. Radiographs of her bilateral upper

extremities on day 6 revealed calcifications in the axillary and brachial arteries as well as in the left radial artery (Appendix Figure 2A). On day 8 of life, she was administered low-dose intravenous pamidronate (0.5 mg/kg/day for 2 days, given every two weeks) and at 3 weeks she was started on low phosphate diet and sevelamer hydrochloride, a phosphate binder. A year later, pamidronate infusion was reduced to 0.5 mg/kg/day once every four weeks and finally discontinued in 2010 after 23 months of treatment. The low phosphate diet and sevelamer hydrochloride were continued until the age of 5.5 years.

At 2 years-of-age, the subject began complaining of pain in her ankles and knees, and started showing signs of bilateral genu valgum. Radiographs revealed multiple growth arrest lines in relation to distal tibia, right fibula, and bilateral knees, however, there were no florid signs of rickets. She displayed pectus carinatum (Appendix Figure 2B). During follow-up examinations at 2.7 years-of-age, echocardiogram revealed a left ventricular shortening fraction of 50% and enhanced echogenicity of the aortic root and ascending aorta. Ultrasound examination of the carotid arteries showed irregular intima of the left carotid artery with no clear signs of calcification, suggesting arterial stenosis at the origin of the left internal carotid artery. By 5 years-of-age, the echogenicity of the aortic and pulmonary vessels had begun to decrease.

On examination at 6.7 years-of-age at the NIH clinical center in 2015, her weight plotted between the 50^{th} and 75^{th} percentiles for her age, while her height was slightly above the 25^{th} percentile. Electrocardiogram (ECG) showed a normal sinus rhythm and her blood pressure was 82/50 mmHg with a heart rate of 90 beats per minute. Echocardiogram showed mildly

thickened mitral valve, aortic valve, and atrial septum. By this age, the most significant cardiovascular calcifications appeared to be resolved, in line with spontaneous regression noted in some previous cases (Ciana et al. 2006). Imaging studies showed faint aortic root calcification as well as calcification along the iliac arteries and right femoral artery. Other pertinent medical findings included predominantly conductive bilateral hearing loss (slight to mild on the right, and mild to moderate on the left) and a history of obstructive sleep apnea resolved after tonsillectomy and adenoidectomy.

Radiographs of lower extremities showed widening of bilateral distal femoral physes with widening of the distal femoral metaphyses, changes compatible with hypophosphatemic rickets (Appendix Figure 2C). Biochemical findings included a history of low-normal inorganic phosphorus or hypophosphatemia, elevated phosphorus in the urine, low 25 dihydroxyvitamin D3, elevated alkaline phosphatase (ALP), undetectable pyrophosphate (PP_i), high-normal parathyroid hormone (PTH), and high fibroblast growth factor 23 (FGF23) (Appendix Table 2). Based on combined clinical, radiological, and biochemical findings, the subject was diagnosed with hypophosphatemic rickets (ARHR2) secondary to GACI (Levy-Litan et al. 2010; Lorenz-Depiereux et al. 2010). She was prescribed 26 ng/kg/d of calcitriol divided in two daily doses, and 30 mg/kg/d of phosphate supplementation divided in four daily doses. A sternal brace was provided to correct her pectus carinatum. Follow-up radiographs after one year of calcitriol and phosphate supplements indicated some positive alterations in femoral physes and metaphyses, with marked improvement in genu valgum (Appendix Figure 2D).

Case 2 Medical History

A 7.11-year-old Caucasian girl (subject 2) with a medical history of GACI, pseudoxanthoma elasticum (PXE; OMIM#264800), attention-deficit/hyperactivity disorder, macrocephaly, cardiomyopathy, renovascular hypertension, and hearing loss was referred to the NIH Clinical Center for GACI and underwent dental evaluation (Figure 1G-K). She was the product of a consanguineous relationship. Subject 2 was born at 34 gestational weeks via Cesarean section, with Apgar score of 6 at one minute and 8 at five minutes. She initially presented with poor respiratory effort, decreased tone, and heart murmurs, and was followed up in the neonatal intensive care unit for 2 weeks. She was placed in the care of her foster parents at 3 weeks-of-age.

At 3 months, subject 2 was admitted to the pediatric intensive care unit for suprasternal retractions and was diagnosed with noncompaction dilated cardiomyopathy and hypertension. In early infancy, the subject had an extensive history of hypertension, calcification in multiple arteries, cardiomyopathy, and hearing loss (Appendix Figure 2E)[previously reported in (Li et al. 2012)]. Since then, she has been closely followed by a cardiologist. Cardiomyopathy, hypertension, and some calcifications spontaneously improved within the first 2 years (Appendix Figure 2F), delaying GACI diagnosis. At age 2, the subject was referred to the dermatology clinic due to skin changes on her neck. A diagnosis of PXE was made based on appearance of pink-yellowish papules coalescing into thin cobblestone plaques distributed circumferentially on the neck and inguinal folds and histological observation of irregular elastic fibers and calcifications in the reticular dermis of a skin biopsy. At this time, the subject was

reported to have an unstable gait, though blood biochemistry results were within normal ranges.

Genetic testing was negative for *ABCC6* mutations (often associated with ectopic calcifications of skin in PXE) but identified two sequence variants in *ENPP1* gene: NM_006208.2:c.517A>C/p.K173Q, a frequent polymorphism considered to be benign, and c.1538A>G/p.Y513C, a pathogenic mutation that has been previously reported in an Italian patient with GACI (Rutsch et al. 2008).

A cardiac CT angiogram with multiplanar and 3-D reformats performed at 2.3 years-of-age revealed calcification of the right atrium, left circumflex artery, and main coronary artery. Magnetic resonance angiogram (MRA) of brain showed a slightly tortuous basilar artery (representative example in Appendix Figure 2G at 7.11 years), and MRA of the neck showed abnormal vertebral arteries. Echocardiogram showed intra-atrial calcifications. At 5 years-of-age, her symptoms had worsened and imaging studies revealed diffuse arterial and bony calcifications, predominantly in her mesenteric, carotid, and vertebral arteries. She began intravenous monthly pamidronate infusions at 0.3-0.5 mg/kg/day. After 1.5 years of treatment, pamidronate was discontinued because of no apparent improvement in vascular calcification. Between 11/2014 and 05/2016 she underwent three mesenteric artery angioplasties. Unfortunately, her arteries re-stenosed and she ultimately underwent aortoceliac bypass and aorto-SMA patch angioplasty in 10/2016.

On examination at 7.11 years-of-age at the NIH clinical center, the diagnosis of GACI with *ENPP1* mutation was confirmed. Her weight was around 95th percentile and height around 89th percentile for her age. ECG showed normal sinus rhythm and her blood pressure was 90/50 mmHg and heart rate 100 beats per minute. Echocardiogram showed dilated left ventricle (LV), severe LV dysfunction with an estimated ejection fraction of 30%, global LV hypokinesis involving the base and mid-ventricle with preserved function of the LV apex area, increased trabeculation and increased echodensity consistent with fibrosis or calcification, significant mitral annular calcification, and calcified aortic valve leaflets with no evidence of substantial aortic stenosis. Abdominal ultrasound showed splenic and renal calcifications with hepatic angioma. Skin examination was notable for papules and nodules in the facial areas consistent with calcinosis cutis. The lesions in the flexural areas were consistent with previous histological diagnosis of PXE. Radiographs showed dystrophic calcification of the left hip and right wrist with no evidence of rickets. Other pertinent medical findings included cervical vertebrae fusion (Appendix Figure 2H), macrocephaly of unknown etiology, bilateral hearing loss (wears hearing aids), ADHD, and renovascular hypertension. Biochemical findings included hypophosphatemia, normal phosphorus in the urine, low 25 dihydroxyvitamin D3, normal ALP, elevated PTH, and normal FGF23 (Appendix Table 2).

Her medication list includes the following: Aspirin 81 mg daily; Clopidogrel 75 mg daily; Enalapril (1 mg/mL) 3 mg twice daily; Propranolol 10 mg twice daily; Amitriptyline 10 mg daily at bedtime; Cetirizine 10 mg daily; Gabapentin 125 mg three times daily; Levetiracetam 900 mg twice daily; Melatonin 3 mg daily at bedtime; Diazepam 2.5 mg PRN; Hydroxyzine 20 mg PRN;

Ibuprofen 300 mg PRN; Oxycodone 3 mg PRN; Tacrolimus topical ointment (0.03%) twice daily PRN; Triamcinolone topical ointment (0.1%) PRN; Lactobacillus Acidophilus 1 tablet daily; Pediatric multivitamin 1 tablet daily.

Case 3 Medical History

A 6.11-year-old Caucasian male (subject 3) with a medical history of GACI, Loeys-Dietz syndrome (LDS; OMIM#609192), hypophosphatemic rickets, periarticular calcification, aortic dilation, arterial tortuosity of the head and neck vessels, chronic lung disease, bilateral retinopathy of prematurity stage 3 (S/P laser surgery), congenital fusion of C3-C4 and C5-C6 vertebral segments, left germinal matrix hemorrhage grade I (resolved), nephrocalcinosis, left inguinal hernia (S/P repair), bilateral moderate mixed hearing loss, and chronic otitis media with effusion, was referred to the NIH Clinical Center for dental evaluation (Figure 1L-P). He was born prematurely to a 29-year-old mother at 25 1/7-weeks of gestation via Caesarean section, with Apgar score of 5 at one minute and 7 at five minutes.

At birth, subject had a prolonged stay in the NICU due to multiple complications of prematurity including prolonged ventilator support, dopamine and hydrocortisone for blood pressure support, and two courses of indomethacin for closure of a Patent Ductus Arteriosus (PDA). He was also found to have a grade I left germinal matrix hemorrhage on day 10 of life, with a subsequent head ultrasound on day 104 of life showing resolution of the bleed, but with mineralizing vasculopathy. He was finally discharged after 118 days of hospitalization.

His parents first noticed a decreased range of motion around shoulders at about 8 months-of-age. An MRI at 1.2 years-of-age revealed bilateral calcified masses (right greater than left) with extension into the biceps sheath and subscapularis recess. Because the calcium deposits were causing significant pain, as well as limitation in the range of motion and delay in developmental milestones, he underwent arthrotomy and debridement. An MRI at 2 years-of-age revealed significantly tortuous and ectatic vertebral and carotid arteries on the right side, although the left side was poorly visualized. Echocardiogram showed aortic root dilatation at 1.97 cm (Z-score 3.14). Given the presence of aortic root dilatation and arterial tortuosity, genetic testing was done, revealing a *TGFBR1* mutation (c.1375C>T; p.Gln459* in exon 8) that was deemed to be consistent with a disease-causing mutation for LDS. Genetic testing of the proband also revealed *ENPP1* compound heterozygous mutations for c.1438T>C (p.Cys480Arg) in exon 15 inherited from the father, and c.2414G>T (p.Gly805Val) in exon 23 inherited from the mother (Figure 1L). It was noted that the father also carried *TGFBR1* mutation similar to the subject. Follow-up evaluation revealed that the father had aortic dilation (requiring aortic root replacement later), intracranial arterial tortuosity, scoliosis, high arch palate, pes planus, and broad shaped uvula, all findings consistent with LDS. The subject's younger sister was also diagnosed with GACI *in utero* and was confirmed to carry the same *ENPP1* mutations, but does not have LDS.

Subject 3 was examined at the NIH clinical center at 6.11 years-of-age. MRI indicated continued presence of calcium deposits in shoulders after arthrotomy and debridement 4 years prior (Appendix Figure 2I, J). Echocardiogram revealed normal ventricular size and function with an

estimated ejection fraction of 60% in left ventricle. Aortic root appeared dilated with a z-score of 3.2. Echocardiogram also revealed narrowing of the ascending aorta (diameter 11 mm) and the aortic walls in this area appear thickened. Also, his ascending aorta appeared to have not grown over the past 3-4 years. There was no evidence of valvular disease or pulmonary hypertension. CT scan showed circumferential calcification involving the ascending aorta, but he has never been treated with bisphosphonates. During his initial evaluation at the NIH three years prior, he showed signs of incipient rickets and was treated subsequently (Appendix Table 2). His medication list included phosphorus 125 mg four times daily; Calcitriol 1 mcg/ml twice daily; Losartan 37.5 mg daily; Guanfacine 1 mg daily; montelukast 5 mg daily; Methylphenidate 5 mg twice daily; Beclomethasone Dipropionate inhaler 2 puffs twice daily; and Polyethylene Glycol 3350. Biochemical findings included low-normal phosphorus, normal phosphorus in the urine, normal ALP, reduced PP_i, normal 25 dihydroxyvitamin D3, normal PTH, and high FGF23 (Appendix Table 2).

Case 4 Medical History

A 26.5-year-old Caucasian female (subject 4) with a history of mild clinical manifestations of GACI, ARHR2, fusion of C2 through C6 vertebral segments, irritable bowel syndrome, and ankle tendonitis was referred to the NIH Clinical Center for GACI and dental evaluation was performed (Figure 2A-E). She was born as a dizygotic twin at 36 to 37 weeks-of-gestation via Caesarean section with Apgar score of 9 at one and five minutes. She is one of three children born to healthy non-consanguineous parents. Her twin brother died at 6 weeks-of-age due to

myocardial infarction, secondary to coronary artery calcification associated with GACI. Her younger sister aged 24 years is reported to be healthy.

Her initial imaging as an infant identified patchy calcification of the abdominal aorta extending down to the bifurcation. A small amount of calcification was evident in her pericardium as well as bronchial and pulmonary arteries. Ultrasound examination at 4 months-of-age revealed faint calcification involving the entire length of the dorsal abdominal aorta. She remained well during infancy and childhood and developed normally. She was never treated with bisphosphonate therapy. By 5 years-of-age, calcification of the bronchial and pulmonary arteries appeared to have resolved. Based on clinical signs and biochemical findings, subject 4 was diagnosed with ARHR2 at the age of 8 and was treated with calcium and phosphate supplements. At 16 years-of-age, a small degree of calcification was noted in the distal part of ascending aorta (Appendix Figure 3A), which has remained stable on subsequent imaging. Her pericardial calcification appeared to have resolved by 22 to 23 years-of-age, with no evidence of recurrence to date. Other recorded manifestations include periarticular calcifications (Appendix Figure 3B).

On examination at the NIH clinical center, the diagnosis of GACI with *ENPP1* mutation was confirmed. Genetic sequencing revealed biallelic *ENPP1* mutations (c.749C>T/p.P250L in exon 7 from father; c.913C>A, p.P305T in exon 8 from mother) (Figure 2A). Subject 4 is one of three children born to healthy non-consanguineous parents (Figure 2B). Despite the same genotype,

variable GACI cardiovascular phenotypes have been described previously in the literature (Cheng et al. 2005; Ciana et al. 2006).

Her ECG showed normal sinus rhythm and her blood pressure was 108/60 mmHg and heart rate 76 beats per minute. Echocardiogram showed structurally normal heart with normal function. Audiological evaluation showed no signs of hearing loss. Radiological evaluation showed fusion of the vertebral bodies and posterior elements C2 through C6 vertebral segments, with narrowing of the AP diameter of the vertebral bodies (Appendix Figure 3C). Radiographs of hand and wrist showed evidence of bony deformity and periarticular calcification. Other pertinent medical findings included irritable bowel syndrome and ankle tendonitis associated with phosphate holiday from 2009 to 2010. Currently, she is being treated for hypophosphatemic rickets with calcitriol and phosphate supplements. Biochemical findings at 26.5 years-of-age included hypophosphatemia, normal phosphorus in the urine, normal ALP, normal 25 dihydroxyvitamin D3, elevated PTH, and elevated FGF23 (Appendix Table 2)

Case 4 Dental History

The early dental history of subject 4 was unremarkable. At 8.9 years, a maxillary first molar (I) appeared infraoccluded (Appendix Figure 7A). Six months later, the molar was severely infraoccluded, dull to percussion (suggesting ankylosis), and a posterior open bite started to develop, prompting extraction of this tooth. She underwent orthodontic treatment between 14-15 years of age, which was reported to be slow and difficult to achieve desired tooth movement. Bitewing x-rays from routine dental examination between 18 and 26-years-of-age

revealed protruding cervical root morphology in maxillary and mandibular molars (Figure 2D, E; Appendix Figure 7B-F). On oral examination, her dentition appeared healthy with no signs of caries or restorations (Figure 2C, Appendix Figure 7G-I). Clinical attachment levels and probing depths were within normal limits, with no signs of inflammation or bleeding on probing (data not shown). She exhibited mild generalized gingival recession secondary to aggressive tooth brushing habit. Furthermore, an unusual "shelf" at the cementum-enamel junction of several teeth was felt during probing.

Case 5 Medical History

A 25.7-year-old Caucasian male (subject 5) with a history of GACI, hypophosphatemic rickets, mitral valve regurgitation, bilateral conductive hearing loss, and bilateral tibial osteotomies for correction of anterior femoral bowing was referred to the NIH Clinical Center for GACI and underwent dental evaluation (Figure 2F-J). He was born at 38 weeks of gestation via normal spontaneous vaginal delivery with Apgar score of 9 at one minute and 10 at five minutes. His 30-year-old half-sister, 22-year-old brother, and non-consanguineous parents were reported to be healthy. His family history includes coronary artery disease, including his maternal second cousin who has two children affected by GACI.

At 29 days, subject 5 started spitting up small amounts of blood and turned blue, and was admitted to the emergency room. On admission, he was blue and dusky in color, and in severe respiratory distress and metabolic acidosis. He was treated with vasopressors and was placed on a ventilator. He improved over the next few days and was discharged after five days of

hospitalization on an apnea monitor. At 48 days, he was again admitted to the emergency room with tachycardia (heart rate of 200), poor peripheral perfusion, systolic murmur, lung crackles, hepatomegaly, and splenomegaly. Chest x-ray revealed cardiomegaly and pulmonary edema. ECG showed ST segment changes and left ventricular hypertrophy. Echocardiogram showed left ventricular enlargement, poor systolic function, and moderate mitral valve regurgitation. Cardiac catheterization showed severe attenuation of the left coronary artery with subtotal occlusion of the first obtuse marginal branch and occlusion proximal to the circumflex branch. The right coronary artery was occluded proximally. CT scan revealed calcification of the descending aorta, renal arteries, splenic artery, superior mesenteric artery, brachial artery, and coronary arteries. A myocardial biopsy was unremarkable, with no evidence of myocarditis.

Genetic testing identified biallelic mutations in *ENPP1* (NM_006208.2: c.1412A>G/p.Y471C in exon 14 inherited from the father and c.1441C>T/p.R481W in exon 15 inherited from the mother). He was diagnosed with GACI and started on intravenous sodium etidronate for seven days, and then placed on oral etidronate at 20 mg/kg/day. During that hospitalization, the echocardiogram improved dramatically, with the left ventricular shortening fraction increasing from 13% on admission to 30% prior to discharge on day 71.

CT scan at 7 months of age showed reduced arterial calcifications, and by 13 months of age the calcifications had regressed completely except for mild calcification of the aortic annulus. Etidronate treatment was discontinued after 24 months-of-age. He remained quite well during

childhood and developed normally. At 13 years-of-age, he complained of pain in the ankles and knees, accompanied by stiffness of both joints. Radiographs revealed significant anterior bowing and thinning of the lower end of both femora (Representative image from 25.7 years old shown in Appendix Figure 3D). A skeletal survey at 14.5-years of age showed resorption of the proximal medial metaphyses of both tibias and widening of the growth plates of the distal ulnae bilaterally, and to a lesser extent, the medial margins of the distal radius. Fusion of the posterior vertebral arches C2-C5 was also found. His ALP level was elevated [631U/L (reference: 166–571 U/L)] and phosphorus level was decreased [2.3 mg/dl (ref: 2.8–5.2mg/dl)]. Based on clinical, laboratory, and radiological findings, he was diagnosed with hypophosphatemic rickets and was treated with calcitriol 0.5 mcg daily and phosphate 250 mg twice daily. Within a few weeks after starting therapy, the pain in his ankles and knees resolved completely. His deformities remained stable, with no progression or improvement. After his final height was achieved, he underwent two separate osteotomies at the age of 21 years to correct the anterior femoral bowing with genu varum (Appendix Figure 3E).

On examination at the NIH clinical center, his height was 163 cm and weight was in the 70th percentile for his age. ECG showed normal sinus rhythm and his blood pressure was 122/62 mmHg and heart rate 76 beats per minute. Echocardiogram showed slow progression of mitral valve regurgitation. CT-scan showed minimal calcifications of the aortic root and inferior portion of the heart with no evidence of pleural or pericardial effusion. Mild calcification was also noted in the posterior and medial papillary muscles (Appendix Figure 3F), and bilateral popliteal arteries. Lateral cervical spine x-ray showed fusion of C2-C5 vertebrae including

vertebral bodies and articular processes. Other pertinent medical findings included mild to moderate bilateral hearing loss (requiring hearing aids), migraines, renal stones (Appendix Figure 3G), and repair of ruptured ankle tendonitis. Currently, he is being treated with calcitriol 0.5 mcg daily and phosphate 500 mg twice daily for hypophosphatemic rickets, lisinopril 10mg once daily for mitral valve regurgitation, and aspirin 81 mg once daily for GACI.

Skin fibroblasts isolated by skin biopsy from subject 5 were tested for ENPP1 enzyme activity, *in vitro*. Compared to control cells, GACI fibroblasts showed a nearly 80% decrease in ENPP1 enzyme activity (Appendix Figure 3H).

Case 5 Dental History

While the subject's early dental history was unremarkable, a class 3 malocclusion with bilateral cross bites was noted and treated with Arnold expanders. Sealants were applied onto at least 9 secondary teeth in his teenage years. Radiographs taken during routine dental examination (17-18-years-old) showed protruding root morphology in premolars and molars, and slightly narrowed root canals in incisors (Appendix Figure 8A-C). Oral examination revealed a relatively healthy dentition with no evidence of caries. A class 1 malocclusion with anterior cross-bite was noted (Figure 2H; Appendix Figure 8D-F). Probing depths and clinical attachment levels were relatively within normal limits with localized areas of gingival recession (data not shown). Mild gingival hyperplasia was noted between maxillary central incisors, which could be related to the ACE inhibitors prescribed for management of mitral valve regurgitation. The unusual root

morphology was confirmed during dental examination (Figure 2I, J; Appendix Figure 8A-C, G, H). Molar cusp patterns had an unusual appearance.

Dental Manifestations in *Enpp1* Mutant Mice

The functional importance of ENPP1 was first investigated in tiptoe walking (*ttw/ttw*) mice, which were found to harbor a spontaneous nonsense mutation in the *Enpp1* gene (Bertrand et al. 2012; Okawa et al. 1998). Additional mutant and knockout mouse models for *Enpp1* exhibited skeletal and biochemical findings consistent with *ttw/ttw Enpp1* mutant mice, including reduced PP_i concentrations, ectopic calcifications (including vascular, soft tissue, and ligament calcification), and hypermineralization of skeletal elements (Anderson et al. 2005; Harmey et al. 2004; Hessle et al. 2002; Johnson et al. 2003; Johnson et al. 2005; Koshizuka et al. 2001; Li et al. 2013; Li et al. 2014; Mackenzie et al. 2012; Narisawa et al. 2007; Okawa et al. 1998). Additional *in vitro* work with a variety of skeletal cells has clarified functions of ENPP1 in production of local extracellular PP_i, as well as upstream regulators of ENPP1 and downstream effects of ENPP1 on cell behavior (Hatch 2007; Hatch and Franceschi 2008; 2009; Hatch et al. 2009; Hatch et al. 2005; Huang et al. 1994; Johnson et al. 2001a; Johnson et al. 2000; Johnson et al. 1999a; Johnson et al. 2001b; Johnson et al. 1999b; Li et al. 2010; Lotz et al. 1995; Solan et al. 1996; Terkeltaub et al. 1994; Vaingankar et al. 2004). *Enpp1* loss-of-function mice also develop biochemical and skeletal manifestations of FGF23-driven hypophosphatemic rickets (Mackenzie et al. 2012).

We previously reported histological findings from both *ttw/ttw* mutant and *Enpp1* knock-out mice, highlighting the rapid growth of cementum to more than 10-fold the thickness of WT mouse acellular cementum (Foster et al. 2012a; Nociti et al. 2002; Zweifler et al. 2015). However, histological approaches used in previous studies were unable to test 3-dimensional changes in acellular and cellular cementum, were not well equipped to identify changes in enamel or dentin, and could not account for alterations in mineral density in any of these tissues. Hence, for the sake of parallel comparison with GACI subjects, we analyzed *Enpp1*$^{asj/asj}$ and WT mouse mandibular molars by high resolution micro-CT, as described in the main text. While *Enpp1*$^{asj/asj}$ mouse acellular cementum exhibited significantly increased thickness and volume, and cellular cementum exhibited significantly increased volume and height (Figure 5), no significant changes were noted in enamel and dentin (Appendix Figure 11).

Histology of *Enpp1*$^{asj/asj}$ mouse molars resembled that of GACI subjects shown in Figure 4. *Enpp1*$^{asj/asj}$ mice featured dramatically expanded cervical cementum (Appendix Figure 12), as previously reported (Foster et al. 2012b; Zweifler et al. 2015). Cementum on the cervical 2/3 of the molar tooth is typically acellular, however in *Enpp1*$^{asj/asj}$ mice this cementum layer features embedded cementocyte-like cells within lacunae.

REFERENCES

Anderson H, Harmey D, Camacho N, Garimella R, Sipe J, Tague S, Bi X, Johnson K, Terkeltaub R, Millán J. 2005. Sustained osteomalacia of long bones despite major improvement in other hypophosphatasia-related mineral deficits in tissue nonspecific alkaline phosphatase/nucleotide pyrophosphatase phosphodiesterase 1 double-deficient mice. Am J Pathol. 166(6):1711-1720.

Benjamini Y, Hochberg Y. 1995. Controlling the false discovery rate - a practical and powerful approach to multiple testing. J Roy Stat Soc B Met. 57(1):289-300.

Bertrand J, Nitschke Y, Fuerst M, Hermann S, Schafers M, Sherwood J, Nalesso G, Ruether W, Rutsch F, Dell'Accio F et al. 2012. Decreased levels of nucleotide pyrophosphatase phosphodiesterase 1 are associated with cartilage calcification in osteoarthritis and trigger osteoarthritic changes in mice. Ann Rheum Dis. 71(7):1249-1253.

Cheng K, Chen M, Ruf N, Lin S, Rutsch F. 2005. Generalized arterial calcification of infancy: Different clinical courses in two affected siblings. American journal of medical genetics Part A. 136(2):210-213.

Ciana G, Trappan A, Bembi B, Benettoni A, Maso G, Zennaro F, Ruf N, Schnabel D, Rutsch F. 2006. Generalized arterial calcification of infancy: Two siblings with prolonged survival. European journal of pediatrics. 165(4):258-263.

Ferreira CR, Ziegler SG, Gupta A, Groden C, Hsu KS, Gahl WA. 2016. Treatment of hypophosphatemic rickets in generalized arterial calcification of infancy (gaci) without worsening of vascular calcification. American journal of medical genetics Part A. 170A(5):1308-1311.

Foster BL, Nagatomo KJ, Nociti FH, Fong H, Dunn D, Tran AB, Wang W, Narisawa S, Millán JL, Somerman MJ. 2012a. Central role of pyrophosphate in acellular cementum formation. PLoS One. 7(6):e38393.

Foster BL, Nagatomo KJ, Nociti FH, Fong H, Dunn DM, Tran AB, Wang W, Narisawa S, Millan JL, Somerman MJ. 2012b. Central role of pyrophosphate in acellular cementum formation. In review.

Glickman ME, Rao SR, Schultz MR. 2014. False discovery rate control is a recommended alternative to bonferroni-type adjustments in health studies. J Clin Epidemiol. 67(8):850-857.

Harmey D, Hessle L, Narisawa S, Johnson K, Terkeltaub R, Millán J. 2004. Concerted regulation of inorganic pyrophosphate and osteopontin by akp2, enpp1, and ank: An integrated model of the pathogenesis of mineralization disorders. Am J Pathol. 164(4):1199-1209.

Hatch NE. 2007. Potential role of pc-1 expression and pyrophosphate elaboration in the molecular etiology of the fgfr-associated craniosynostosis syndromes. Orthod Craniofac Res. 10(2):53-58.

Hatch NE, Franceschi RT. 2008. Fgf2 induced expression of the pyrophosphate generating enzyme, pc-1, is mediated by runx2 and msx2. J Musculoskelet Neuronal Interact. 8(4):318-320.

Hatch NE, Franceschi RT. 2009. Osteoblast differentiation stage-specific expression of the pyrophosphate-generating enzyme pc-1. Cells Tissues Organs. 189(1-4):65-69.

Hatch NE, Li Y, Franceschi RT. 2009. Fgf2 stimulation of the pyrophosphate-generating enzyme, pc-1, in pre-osteoblast cells is mediated by runx2. J Bone Miner Res. 24(4):652-662.
Hatch NE, Nociti F, Swanson E, Bothwell M, Somerman M. 2005. Fgf2 alters expression of the pyrophosphate/phosphate regulating proteins, pc-1, ank and tnap, in the calvarial osteoblastic cell line, mc3t3e1(c4). Connect Tissue Res. 46(4-5):184-192.
Hessle L, Johnson K, Anderson H, Narisawa S, Sali A, Goding J, Terkeltaub R, Millan J. 2002. Tissue-nonspecific alkaline phosphatase and plasma cell membrane glycoprotein-1 are central antagonistic regulators of bone mineralization. Proc Natl Acad Sci U S A. 99(14):9445-9449.
Huang R, Rosenbach M, Vaughn R, Provvedini D, Rebbe N, Hickman S, Goding J, Terkeltaub R. 1994. Expression of the murine plasma cell nucleotide pyrophosphohydrolase pc-1 is shared by human liver, bone, and cartilage cells. Regulation of pc-1 expression in osteosarcoma cells by transforming growth factor-beta. J Clin Invest. 94(2):560-567.
Jansen RS, Duijst S, Mahakena S, Sommer D, Szeri F, Varadi A, Plomp A, Bergen AA, Oude Elferink RP, Borst P et al. 2014. Abcc6-mediated atp secretion by the liver is the main source of the mineralization inhibitor inorganic pyrophosphate in the systemic circulation-brief report. Arterioscler Thromb Vasc Biol. 34(9):1985-1989.
Jansen S, Perrakis A, Ulens C, Winkler C, Andries M, Joosten RP, Van Acker M, Luyten FP, Moolenaar WH, Bollen M. 2012. Structure of npp1, an ectonucleotide pyrophosphatase/phosphodiesterase involved in tissue calcification. Structure. 20(11):1948-1959.
Johnson K, Goding J, Van Etten D, Sali A, Hu SI, Farley D, Krug H, Hessle L, Millan JL, Terkeltaub R. 2003. Linked deficiencies in extracellular pp(i) and osteopontin mediate pathologic calcification associated with defective pc-1 and ank expression. J Bone Miner Res. 18(6):994-1004.
Johnson K, Hashimoto S, Lotz M, Pritzker K, Goding J, Terkeltaub R. 2001a. Up-regulated expression of the phosphodiesterase nucleotide pyrophosphatase family member pc-1 is a marker and pathogenic factor for knee meniscal cartilage matrix calcification. Arthritis Rheum. 44(5):1071-1081.
Johnson K, Hessle L, Vaingankar S, Wennberg C, Mauro S, Narisawa S, Goding J, Sano K, Millan J, Terkeltaub R. 2000. Osteoblast tissue-nonspecific alkaline phosphatase antagonizes and regulates pc-1. Am J Physiol Regul Integr Comp Physiol. 279(4):R1365-1377.
Johnson K, Moffa A, Chen Y, Pritzker K, Goding J, Terkeltaub R. 1999a. Matrix vesicle plasma cell membrane glycoprotein-1 regulates mineralization by murine osteoblastic mc3t3 cells. J Bone Miner Res. 14(6):883-892.
Johnson K, Polewski M, van Etten D, Terkeltaub R. 2005. Chondrogenesis mediated by ppi depletion promotes spontaneous aortic calcification in npp1-/- mice. Arterioscler Thromb Vasc Biol. 25(4):686-691.
Johnson K, Pritzker K, Goding J, Terkeltaub R. 2001b. The nucleoside triphosphate pyrophosphohydrolase isozyme pc-1 directly promotes cartilage calcification through chondrocyte apoptosis and increased calcium precipitation by mineralizing vesicles. J Rheumatol. 28(12):2681-2691.
Johnson K, Vaingankar S, Chen Y, Moffa A, Goldring M, Sano K, Jin-Hua P, Sali A, Goding J, Terkeltaub R. 1999b. Differential mechanisms of inorganic pyrophosphate production by

plasma cell membrane glycoprotein-1 and b10 in chondrocytes. Arthritis Rheum. 42(9):1986-1997.
Koshizuka Y, Ikegawa S, Sano M, Nakamura K, Nakamura Y. 2001. Isolation of novel mouse genes associated with ectopic ossification by differential display method using ttw, a mouse model for ectopic ossification. Cytogenet Cell Genet. 94(3-4):163-168.
Levy-Litan V, Hershkovitz E, Avizov L, Leventhal N, Bercovich D, Chalifa-Caspi V, Manor E, Buriakovsky S, Hadad Y, Goding J et al. 2010. Autosomal-recessive hypophosphatemic rickets is associated with an inactivation mutation in the enpp1 gene. Am J Hum Genet. 86(2):273-278.
Li Q, Guo H, Chou DW, Berndt A, Sundberg JP, Uitto J. 2013. Mutant enpp1asj mice as a model for generalized arterial calcification of infancy. Dis Model Mech. 6(5):1227-1235.
Li Q, Pratt CH, Dionne LA, Fairfield H, Karst SY, Sundberg JP, Uitto J. 2014. Spontaneous asj-2j mutant mouse as a model for generalized arterial calcification of infancy: A large deletion/insertion mutation in the enpp1 gene. PLoS One. 9(12):e113542.
Li Q, Schumacher W, Jablonski D, Siegel D, Uitto J. 2012. Cutaneous features of pseudoxanthoma elasticum in a patient with generalized arterial calcification of infancy due to a homozygous missense mutation in the enpp1 gene. Br J Dermatol. 166(5):1107-1111.
Li Y, Liu J, Hudson M, Kim S, Hatch NE. 2010. Fgf2 promotes msx2 stimulated pc-1 expression via frs2/mapk signaling. J Cell Biochem. 111(5):1346-1358.
Lomashvili KA, Khawandi W, O'Neill WC. 2005. Reduced plasma pyrophosphate levels in hemodialysis patients. J Am Soc Nephrol. 16(8):2495-2500.
Lorenz-Depiereux B, Schnabel D, Tiosano D, Häusler G, Strom T. 2010. Loss-of-function enpp1 mutations cause both generalized arterial calcification of infancy and autosomal-recessive hypophosphatemic rickets. Am J Hum Genet. 86(2):267-272.
Lotz M, Rosen F, McCabe G, Quach J, Blanco F, Dudler J, Solan J, Goding J, Seegmiller J, Terkeltaub R. 1995. Interleukin 1 beta suppresses transforming growth factor-induced inorganic pyrophosphate (ppi) production and expression of the ppi-generating enzyme pc-1 in human chondrocytes. Proc Natl Acad Sci U S A. 92(22):10364-10368.
Mackenzie NC, Zhu D, Milne EM, van 't Hof R, Martin A, Quarles DL, Millán JL, Farquharson C, MacRae VE. 2012. Altered bone development and an increase in fgf-23 expression in enpp1(-/-) mice. PLoS One. 7(2):e32177.
Narisawa S, Harmey D, Yadav M, O'Neill W, Hoylaerts M, Millán J. 2007. Novel inhibitors of alkaline phosphatase suppress vascular smooth muscle cell calcification. J Bone Miner Res. 22(11):1700-1710.
Nociti FJ, Berry J, Foster B, Gurley K, Kingsley D, Takata T, Miyauchi M, Somerman M. 2002. Cementum: A phosphate-sensitive tissue. Journal of dental research. 81(12):817-821.
Normand J, Karasek MA. 1995. A method for the isolation and serial propagation of keratinocytes, endothelial cells, and fibroblasts from a single punch biopsy of human skin. In Vitro Cell Dev Biol Anim. 31(6):447-455.
Okawa A, Nakamura I, Goto S, Moriya H, Nakamura Y, Ikegawa S. 1998. Mutation in npps in a mouse model of ossification of the posterior longitudinal ligament of the spine. Nat Genet. 19(3):271-273.

Ramnitz MS, Gourh P, Goldbach-Mansky R, Wodajo F, Ichikawa S, Econs MJ, White KE, Molinolo A, Chen MY, Heller T et al. 2016. Phenotypic and genotypic characterization and treatment of a cohort with familial tumoral calcinosis/hyperostosis-hyperphosphatemia syndrome. Journal of bone and mineral research : the official journal of the American Society for Bone and Mineral Research. 31(10):1845-1854.

Ruf N, Uhlenberg B, Terkeltaub R, Nürnberg P, Rutsch F. 2005. The mutational spectrum of enpp1 as arising after the analysis of 23 unrelated patients with generalized arterial calcification of infancy (gaci). Human mutation. 25(1):98.

Rutsch F, Böyer P, Nitschke Y, Ruf N, Lorenz-Depierieux B, Wittkampf T, Weissen-Plenz G, Fischer R, Mughal Z, Gregory J et al. 2008. Hypophosphatemia, hyperphosphaturia, and bisphosphonate treatment are associated with survival beyond infancy in generalized arterial calcification of infancy. Circ Cardiovasc Genet. 1(2):133-140.

Solan J, Deftos L, Goding J, Terkeltaub R. 1996. Expression of the nucleoside triphosphate pyrophosphohydrolase pc-1 is induced by basic fibroblast growth factor (bfgf) and modulated by activation of the protein kinase a and c pathways in osteoblast-like osteosarcoma cells. J Bone Miner Res. 11(2):183-192.

Stella J, Buers I, van de Wetering K, Hohne W, Rutsch F, Nitschke Y. 2016. Effects of different variants in the enpp1 gene on the functional properties of ectonucleotide pyrophosphatase/phosphodiesterase family member 1. Human mutation. 37(11):1190-1201.

Terkeltaub R, Rosenbach M, Fong F, Goding J. 1994. Causal link between nucleotide pyrophosphohydrolase overactivity and increased intracellular inorganic pyrophosphate generation demonstrated by transfection of cultured fibroblasts and osteoblasts with plasma cell membrane glycoprotein-1. Relevance to calcium pyrophosphate dihydrate deposition disease. Arthritis Rheum. 37(6):934-941.

Vaingankar S, Fitzpatrick T, Johnson K, Goding J, Maurice M, Terkeltaub R. 2004. Subcellular targeting and function of osteoblast nucleotide pyrophosphatase phosphodiesterase 1. Am J Physiol Cell Physiol. 286(5):C1177-1187.

Zweifler LE, Patel MK, Nociti FH, Jr., Wimer HF, Millan JL, Somerman MJ, Foster BL. 2015. Counter-regulatory phosphatases tnap and npp1 temporally regulate tooth root cementogenesis. Int J Oral Sci. 7(1):27-41.

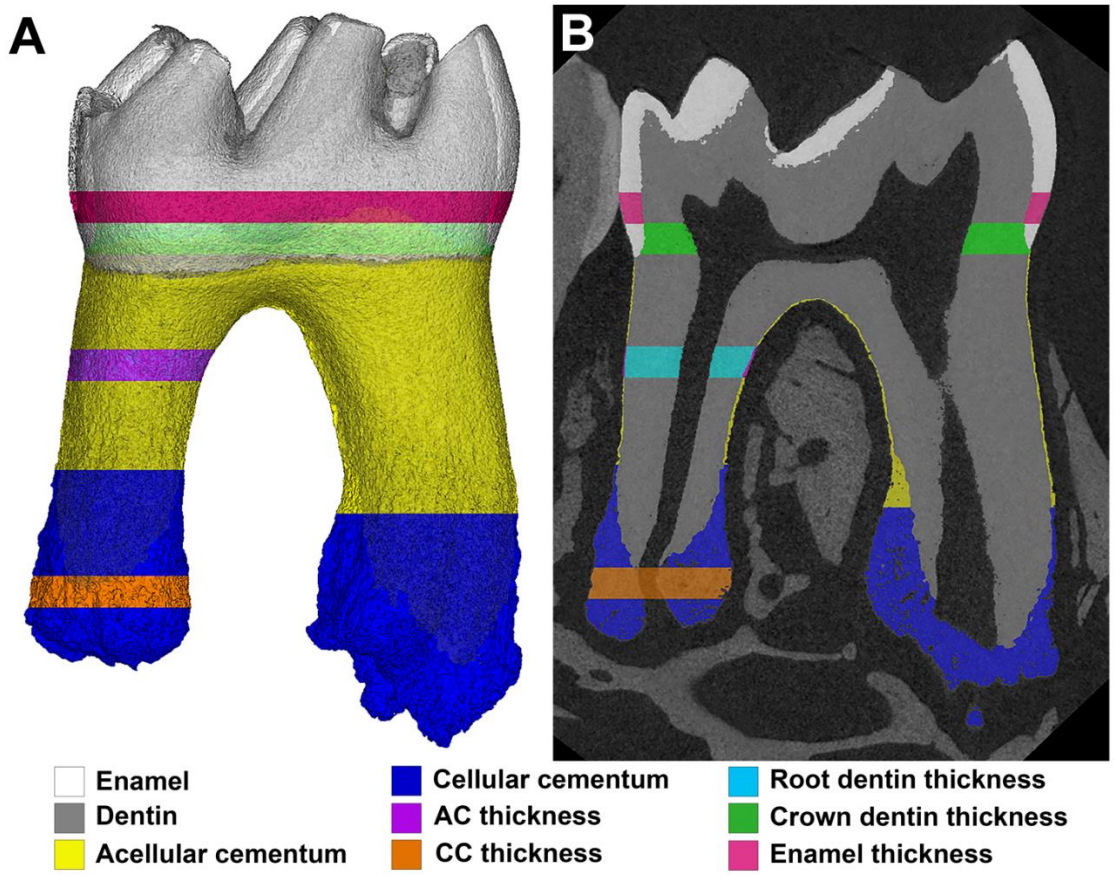

Appendix Figure 1. Micro-computed tomography analysis of mouse molars. The oriented mouse molar tooth is shown in 3D render (left image) and 2D cut plane (right image), with regions of interest (ROI) used for tissue analysis color coded and described in the key. Enamel is shown in white, dentin in grey, acellular cementum in yellow, and cellular cementum in dark blue. Tissue volumes were determined using entire 3D volumes of segmented tissues. Enamel thickness (pink ROI) was determined by measuring 100 µm (50 slices) of enamel located 100 µm coronal to the cementum-enamel junction (CEJ). Crown dentin thickness (green ROI) was determined by measuring 100 µm (50 slices) of dentin directly coronal to the CEJ. Root dentin thickness of the mesial root (light blue ROI) was determined by measuring 100 µm (50 slices) of dentin located 1/3 of the distance from CEJ to root apex. Acellular cementum thickness (purple

ROI) was determined by measuring 100 µm (50 slices) of cementum located 1/3 of the distance from CEJ to root apex. Cellular cementum thickness (orange ROI) was determined by measuring 100 µm (50 slices) of cementum apical to the termination of root dentin.

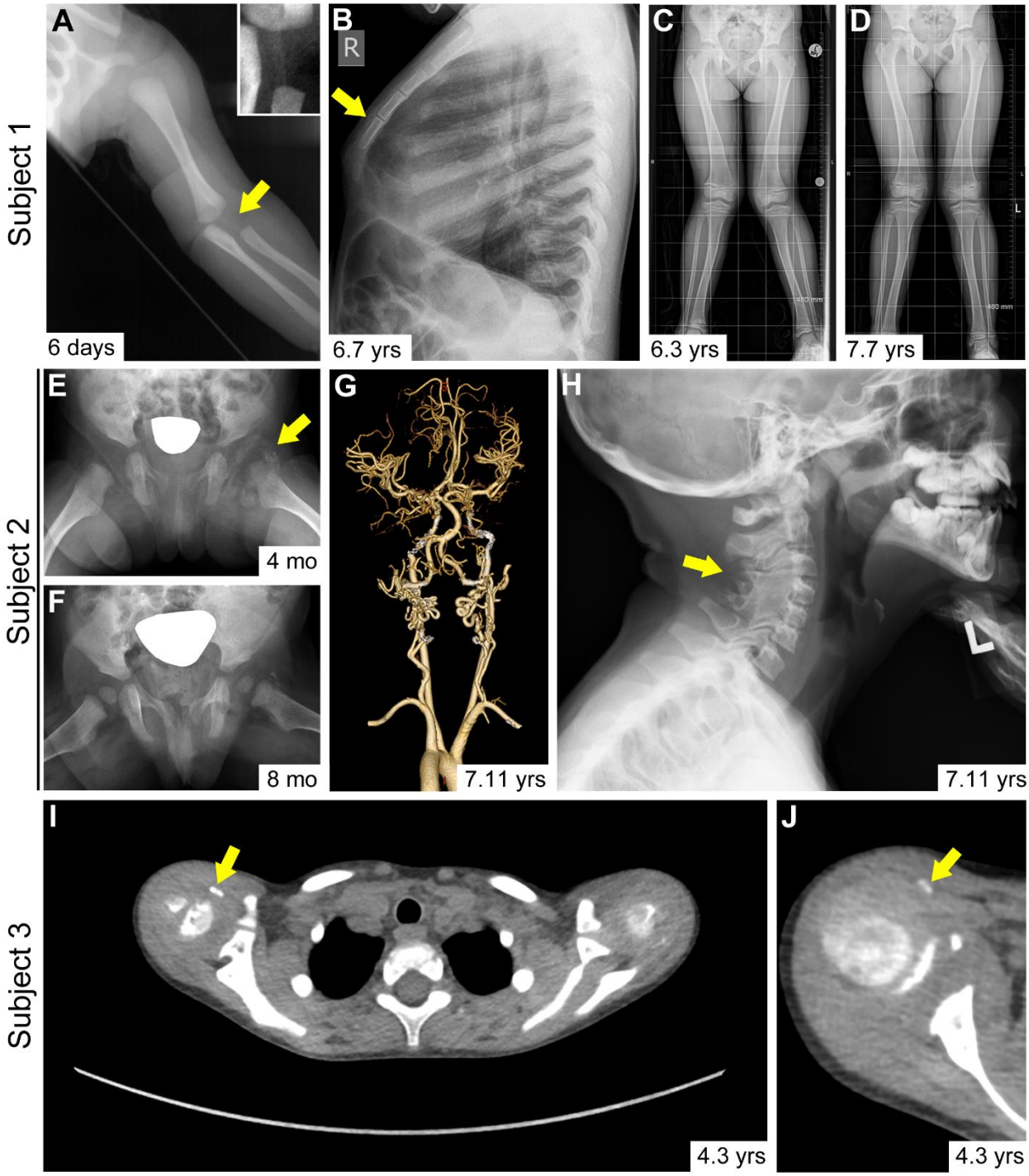

Appendix Figure 2. Clinical manifestations of GACI in subjects 1-3. (A-D) Representative manifestations of GACI for subject 1 are shown for ages 6 days to 7.7 years (yrs). **(A)** On day 6 after birth, calcification in the left radial artery was observed by radiograph (yellow arrow).

Inset shows zoom in of the radiopaque area of the vessel. **(B)** Subject 1 exhibited anteriorly protruding sternum indicative of pectus carinatum, a sign of hypophosphatemic rickets. **(C)** Radiograph of lower extremities at 6.3 yrs shows severe genu valgum and widening of distal femoral physes with widening of the distal femoral metaphyses, signs of rickets. **(D)** By 7.7 yrs, after one year of calcitriol and phosphate treatment, subject 1 exhibited improvements in femurs and reduced severity of genu valgum. (E-H) Representative manifestations of GACI for subject 2 are shown for ages 4 months (mo) to 7.7 yrs. **(E)** At 4 mo, subject 2 exhibited significant ectopic calcification adjacent to right femoral head (yellow arrow), though **(F)** calcification in this region had largely resolved by 8 mo. **(G)** Magnetic resonance angiogram of brain showing tortuous basilar artery. **(H)** By radiological evaluation at 7.11 yrs, subject 2 showed fusion of the vertebral bodies and posterior elements C2 through C6 vertebral segments (yellow arrow), with narrowing of the AP diameter of the vertebral bodies. (I-J) Representative manifestations of ectopic calcifications for subject 3 are shown at age 4.3 yrs. **(I, J)** Subject 3 exhibited calcium deposits in bilateral upper extremities (yellow arrows), where right shoulder calcifications are shown at higher magnification in panel J.

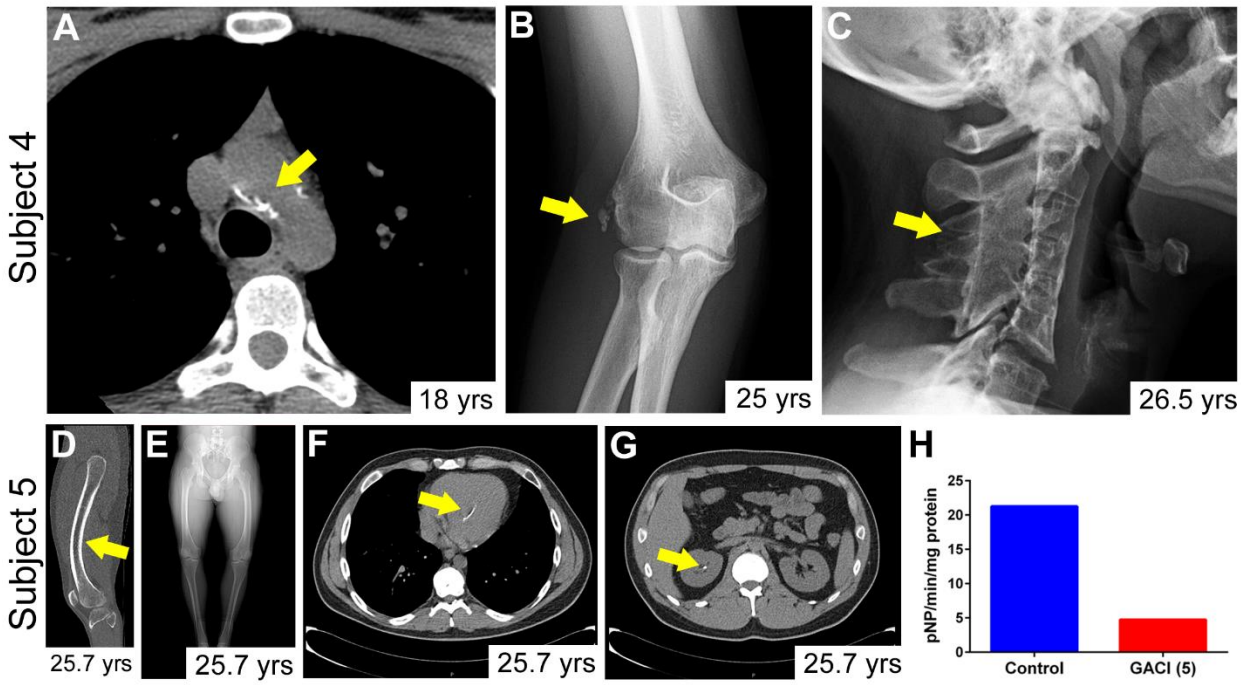

Appendix Figure 3. Clinical manifestations of GACI in subjects 4 and 5. (A) At 18 yrs, subject 4 exhibited a small degree of calcification in the distal part of ascending aorta (yellow arrow). **(B)** Periarticular calcifications near the elbow of subject 4 at 25 yrs. **(C)** By 26.5 yrs, subject 4 displayed fusion of the vertebral bodies and posterior elements C2 through C6 vertebral segments (yellow arrow), with narrowing of the AP diameter of the vertebral bodies. (D-H) Representative manifestations of GACI for subject 5 are shown at 25.7 yrs. **(D)** Anterior bowing of femur (yellow arrow). **(E)** Radiograph of lower extremities showed mild genu varum following osteotomies. **(F)** Mild calcification (yellow arrow) was observed in the papillary muscles of subject 5. **(G)** Renal stones (yellow arrow) were observed in kidneys of subject 5. **(H)** Skin fibroblasts isolated from subject 5 show a nearly 80% decrease in ENPP1 enzyme activity *in vitro* compared to healthy control fibroblasts.

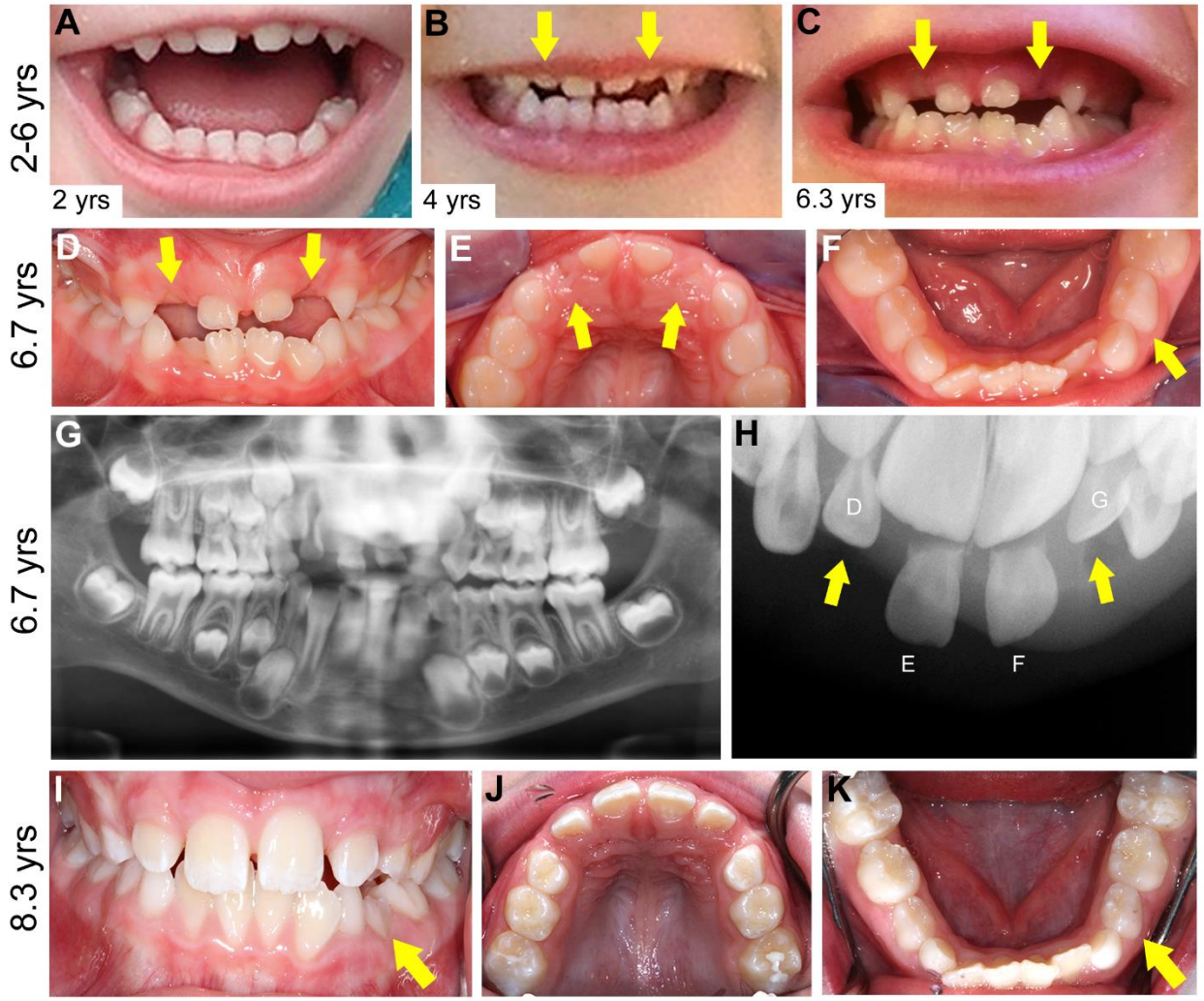

Appendix Figure 4. Additional dental history of GACI subject 1. (A-C) Photographs taken of GACI subject 1 from 2 to 6-years-of-age document progressive infraocclusion of maxillary lateral incisors (yellow arrows). The first photograph taken at age 2 years (yrs) shows normally erupted incisors. In the second photograph, taken 2 yrs later, the subject exhibits partially infraoccluded incisors. By 6.3 yrs, incisors are completely infroccluded beneath the gingiva. **(D-F)** Clinical photographs at 6.7-years-of-age reveal infraoccluded primary maxillary lateral incisors (yellow arrows) and mild-moderate infraocclusion of mandibular primary first molar L (yellow arrow in F). **(G)** Panoramic radiograph reveals normal mixed dentition at 6.7 yrs. **(H)**

Periapical radiograph reveals infraoccluded lateral incisors (D, G; yellow arrows) in the maxilla. **(I-K)** At 8.3 yrs, following extraction of primary maxillary canines and lateral incisors, secondary maxillary lateral incisors are now erupted. However, left mandibular first molar (L) is infraoccluded (yellow arrow in panels I and K) with developing open bite.

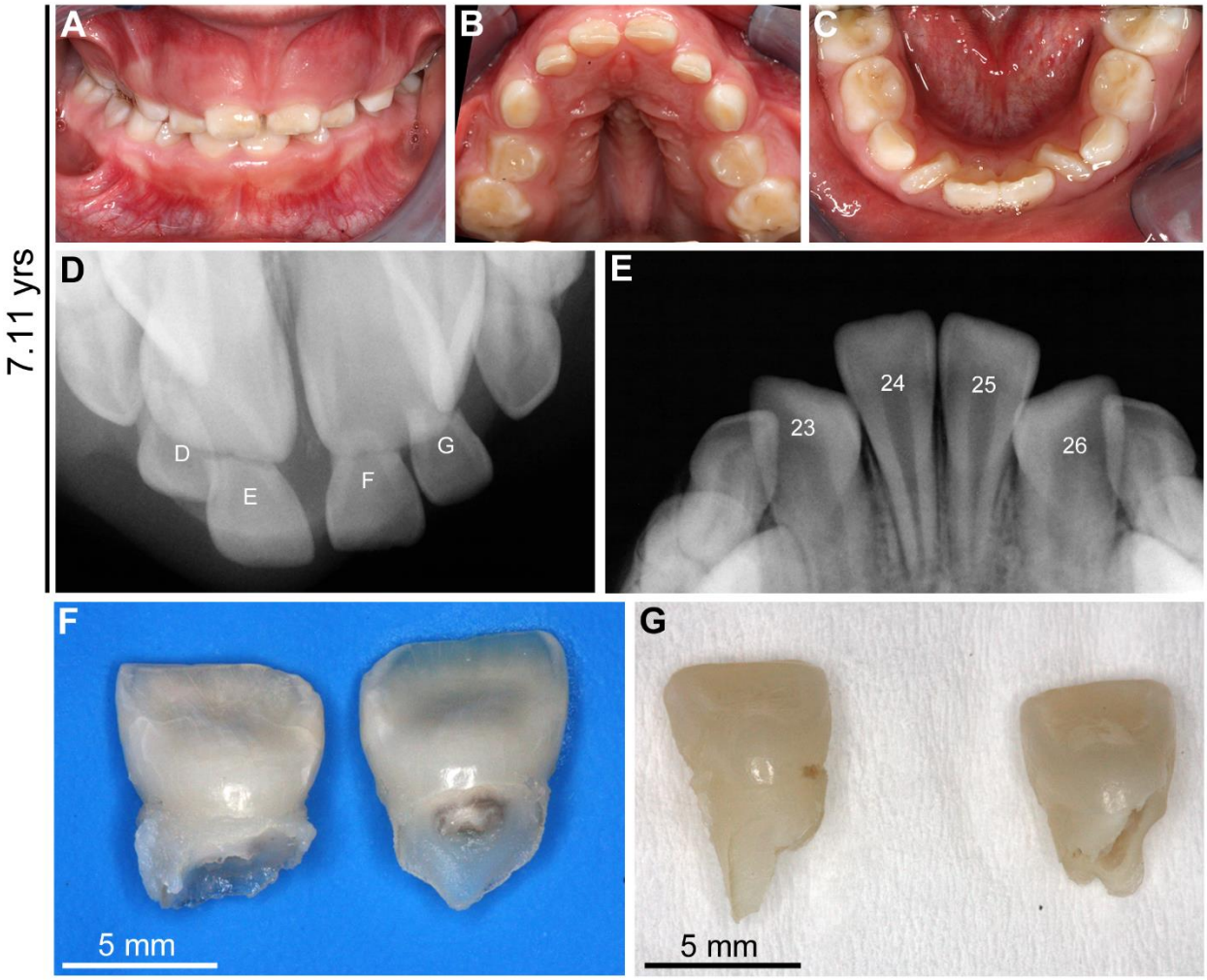

Appendix Figure 5. Additional dental history of GACI subject 2. (A-C) Clinical photographs of subject 2 at 7.11-years-of-age (yrs) reveal a mixed dentition with gingival hyperplasia and mild discoloration in enamel of central incisors. **(D)** Dental radiograph indicate over-retained maxillary central and lateral incisors. **(E)** Radiographs of mandibular incisors indicate rotated lateral incisors (23, 26) with an unusual contour at the CEJ. **(F)** Central and **(G)** lateral primary maxillary incisors extracted from subject 2 exhibit expanded and rough root surfaces.

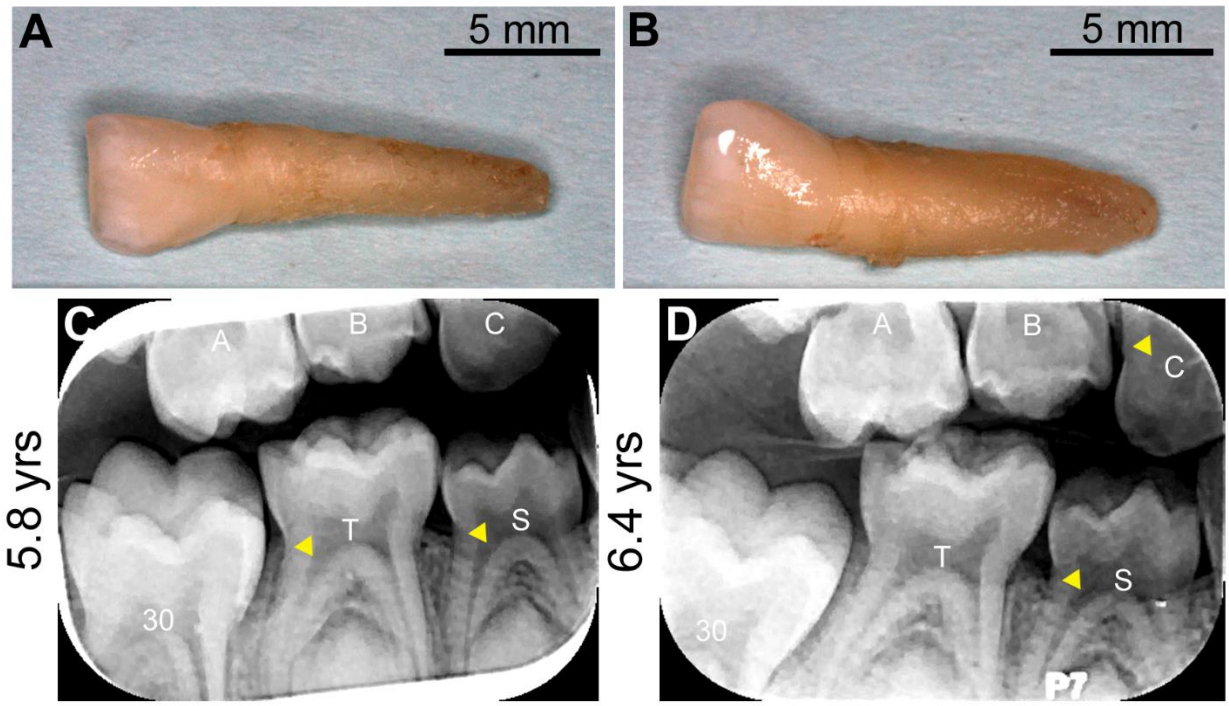

Appendix Figure 6. Additional dental history of GACI subject 3. (A, B) Primary lateral mandibular incisors extracted from subject 3 at 6.3 yrs show substantial remaining root structure. Bitewing radiographs of subject 3 at **(C)** 5.8 and **(D)** 6.4 years (yrs) showing subtle expansion of root contour (yellow arrowheads) at the cementum-enamel junctions of some teeth.

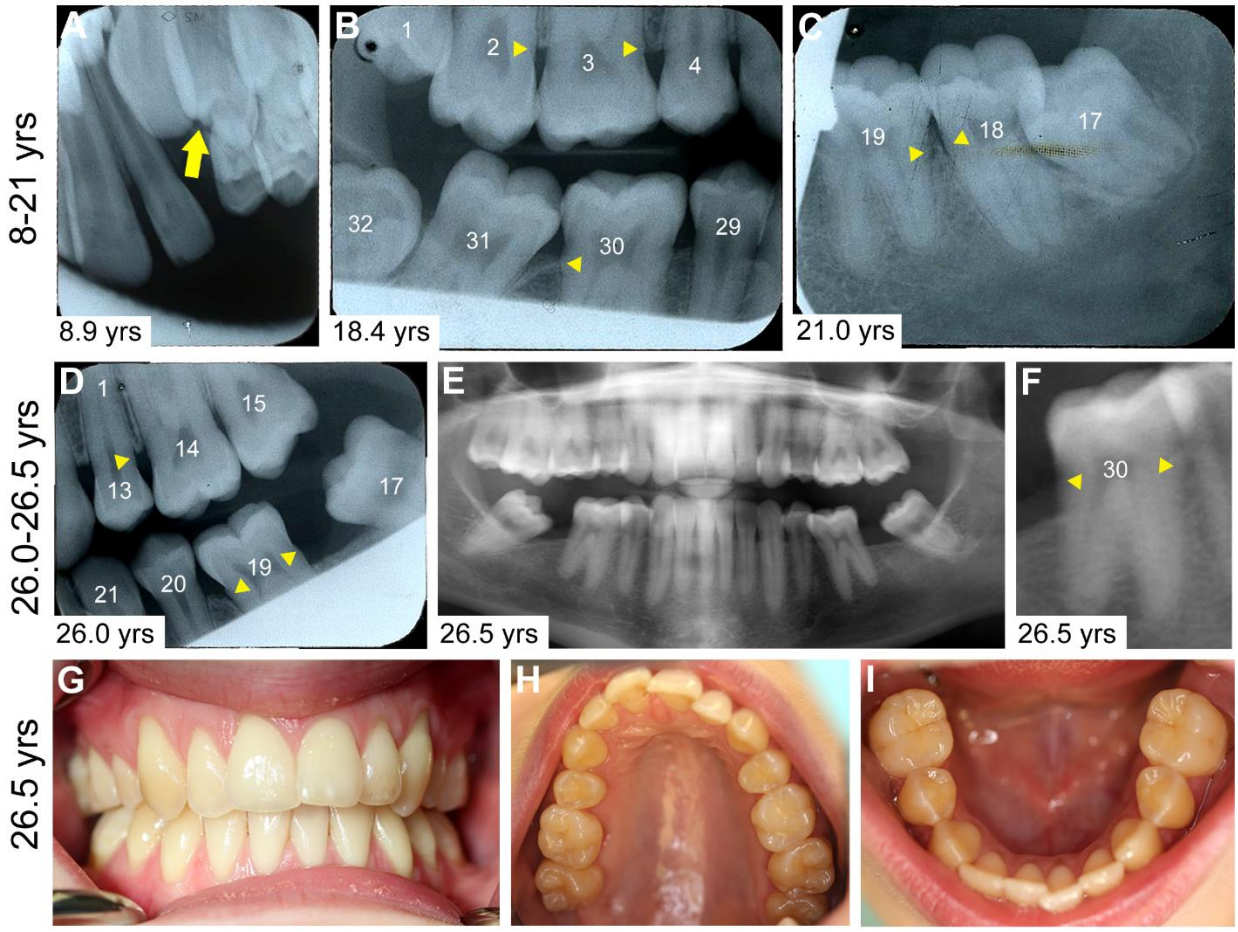

Appendix Figure 7. Additional dental history of GACI subject 4. (A) Dental bitewing radiograph at 8.9 years (yrs) shows infraoccluded primary maxillary molar (I; yellow arrow). Dental bitewing radiographs at **(B)** 18.4 yrs and **(C)** 21.0 yrs exhibit protruding root morphologies (yellow arrowheads) on premolars and molars. **(D)** Dental bitewing radiograph at 26.0 yrs shows protruding cervical root morphology (yellow arrowheads) in premolars and molars. **(E)** Panoramic radiograph at 26.5 yrs showing normal adult dentition. Root morphology is difficult to discern in panoramic radiographs, but **(F)** zoomed in images of mandibular molars (e.g., 30 shown here) suggest an unusual bulging contour in the cervical roots of these teeth. **(G-I)** Oral photographs at 26.5-years-of-age reveal a healthy dentition, absence of caries, with generalized gingival recession.

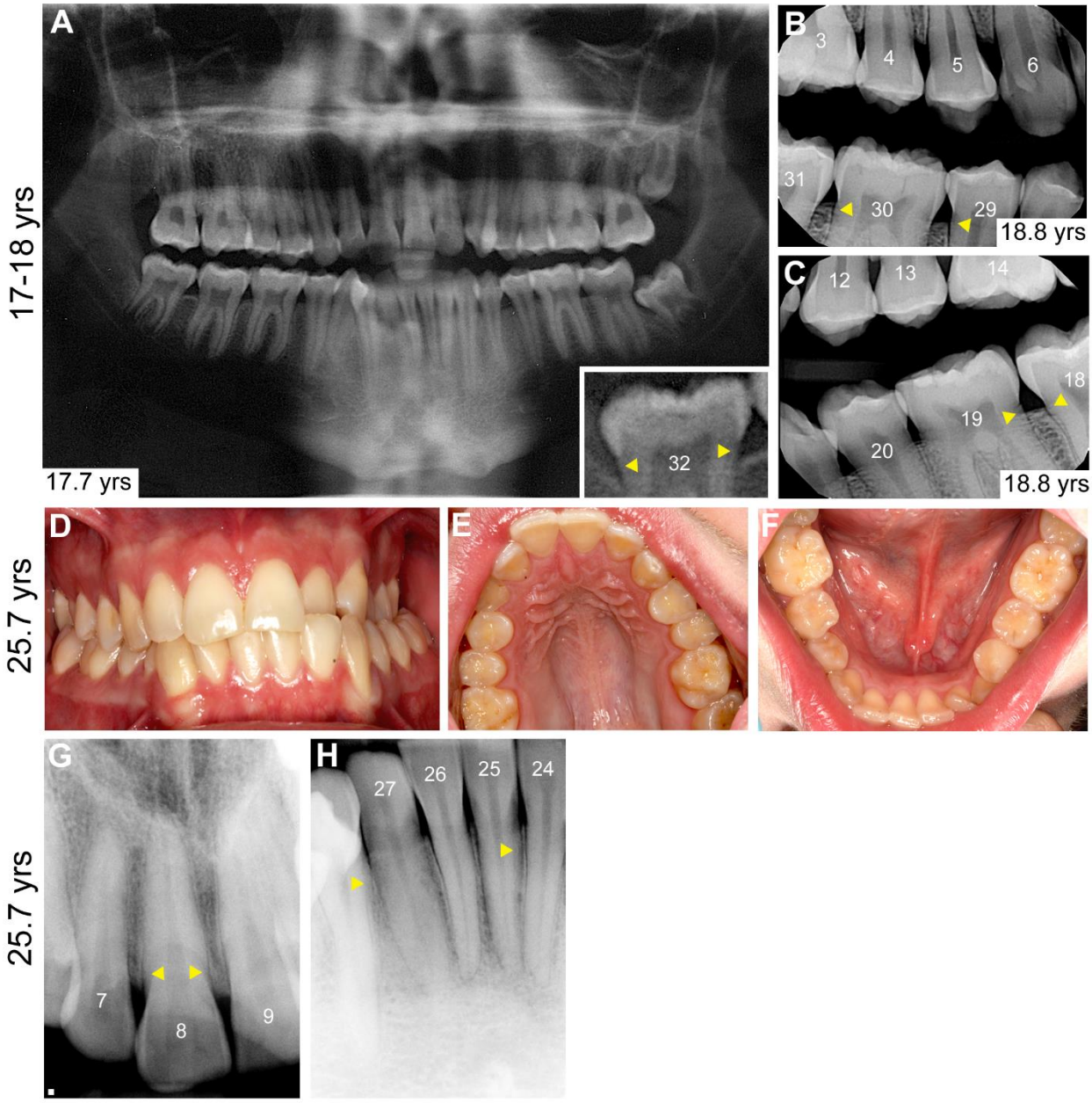

Appendix Figure 8. Additional dental history of GACI subject 5. (A) Panoramic radiograph at 17.7 years (yrs) showing a normal adult dentition. When molar teeth are examined carefully, expanded root morphology can be discerned (yellow arrowheads in inset). **(B, C)** Dental bitewing radiographs at 18.8 yrs exhibit protruding root morphologies (yellow arrowheads) on premolars and molars. **(D-F)** Oral photographs show a healthy dentition with no evidence of

caries, a class 1 malocclusion anterior cross-bite, and unusual molar cusp patterns. **(G, H)** Dental bitewing radiographs at 25.7 yrs exhibit generally normal anterior teeth, with some subtle unusual root morphologies (yellow arrowheads).

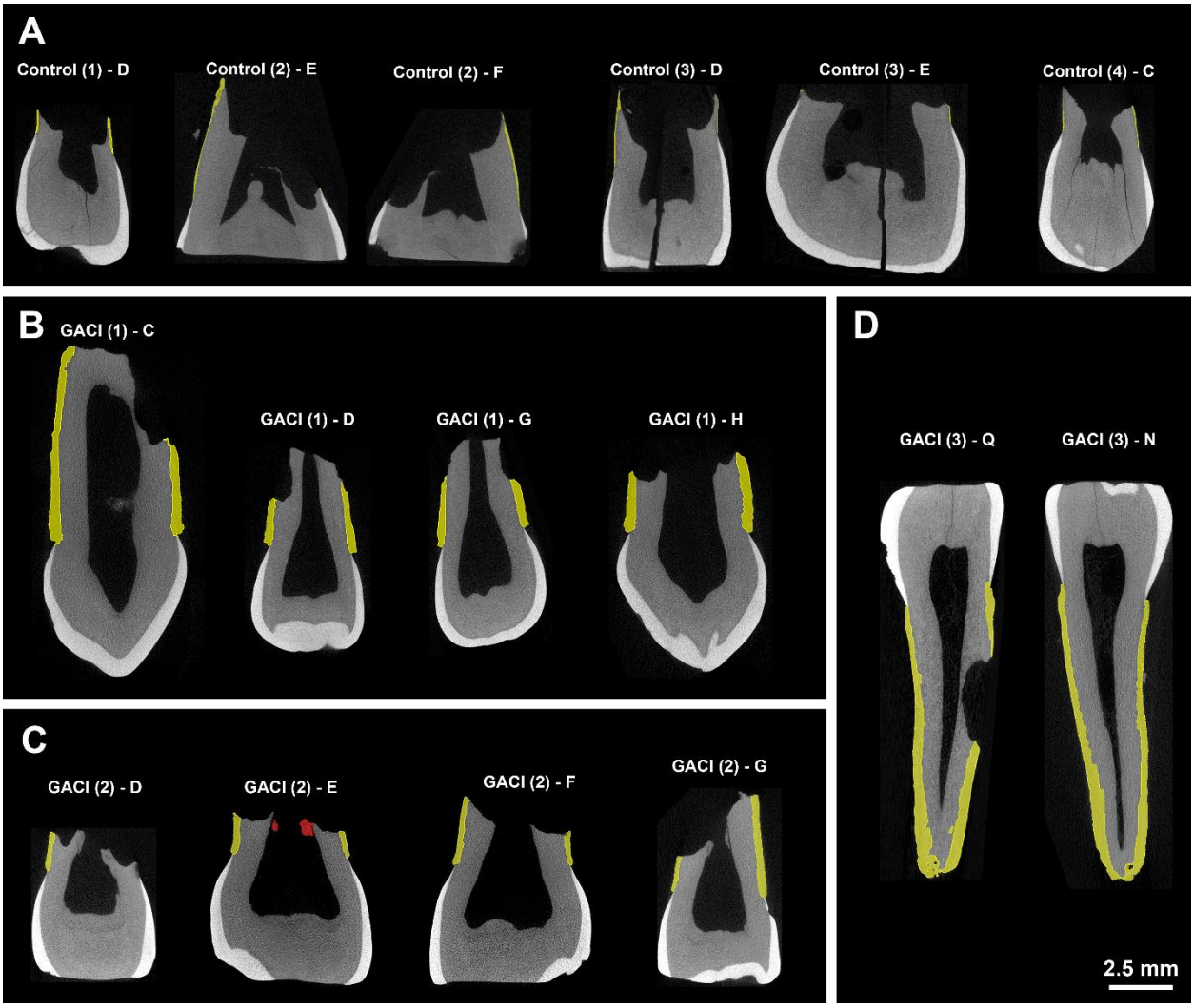

Appendix Figure 9. Analysis of healthy control and GACI teeth. Panel of 2D micro-computed tomography images of exfoliated and extracted teeth from **(A)** 4 control subjects and **(B-D)** 3 GACI subjects. Teeth are identified by subject and letter. Enamel is shown in white, dentin is shown in gray, and the cementum layer is represented in yellow.

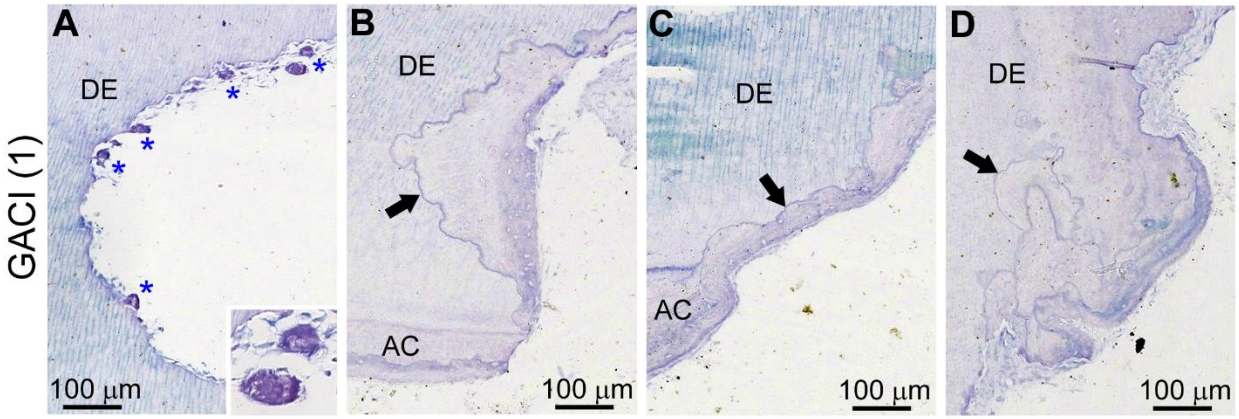

Appendix Figure 10. Distribution of osteoclast/odontoclast-like cells on teeth from GACI subjects. Panels A-D show histological sections stained for tartrate-resistant acid phosphatase (TRAP), a marker of osteoclast/odontoclast cells. Representative sections are shown from GACI subject 1 maxillary canine (A and C) and lateral incisor (B and D). **(A)** Some regions of GACI teeth exhibit numerous osteoclast/osontoclast-like cells (blue asterisks; shown at increased magnification in the inset) in association with Howship's lacunae on dentin (DE) surfaces, as expected for actively resorbing regions of primary teeth undergoing exfoliation. **(B-D)** In contrast, some regions of GACI teeth exhibit evidence of past resorption, though no TRAP-positive osteoclast/odontoclast-like cells are evident. Progress of resorption appears to have been arrested, and Howship's lacunae have been filled with new cellular cementum-like tissues (black arrows).

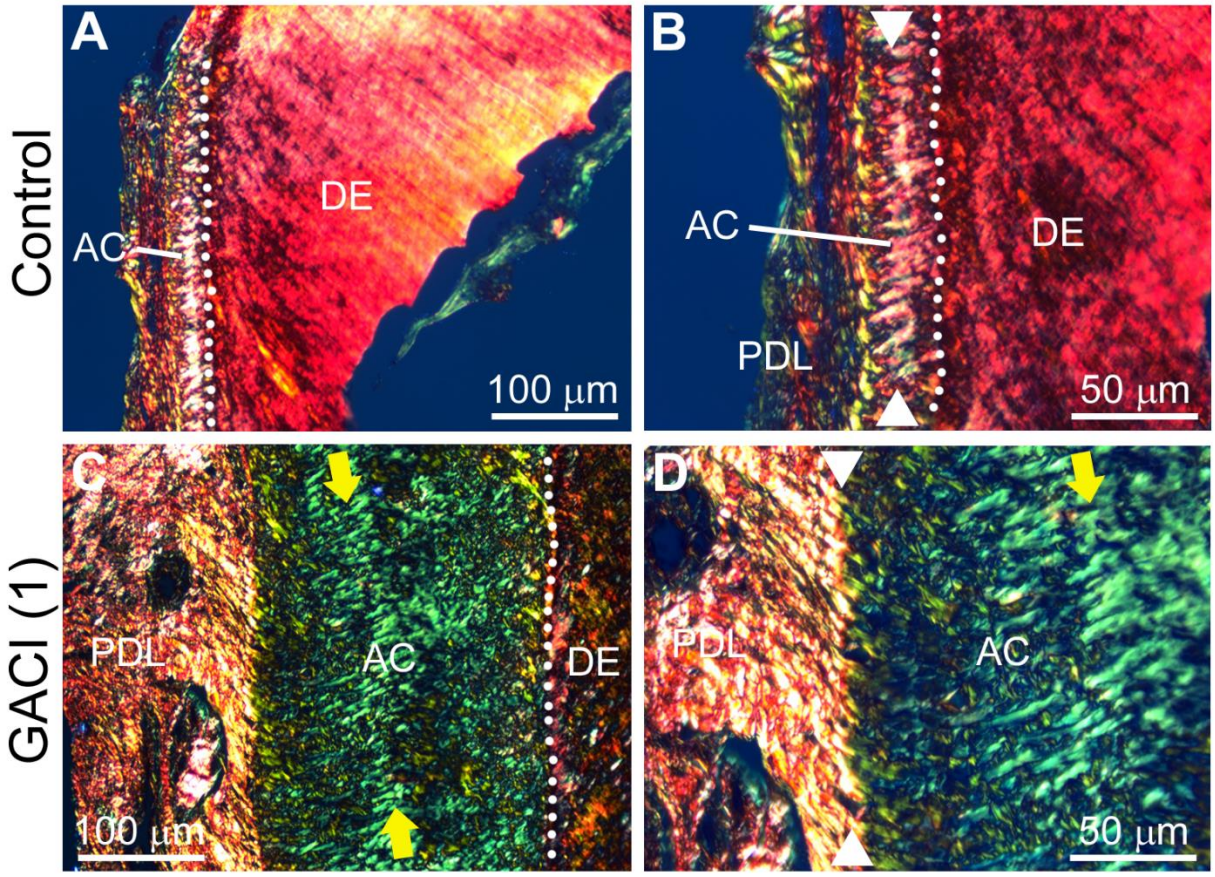

Appendix Figure 11. Polarized light microscopy of cementum in teeth from GACI and control subjects. Histological sections of control incisor and GACI canine were stained by picrosirius red dye and observed under polarized light microscopy to visualize collagen fiber organization. **(A, B)** Control incisor displays typical organization of collagen fibers within the acellular cementum (AC) layer, visualized as densely embedded fibers (between white arrowheads in B) perpendicular to cementum-periodontal ligament (PDL) surface. White dotted line is included to mark the location of the AC-dentin (DE) interface. **(C, D)** GACI canine displays highly organized collagen fibers throughout its expanded thickness (for example, see yellow arrows in C and D), as well as extrinsic fibers enter AC at the PDL interface (between white arrowheads in D). White dotted line in C is included to mark the location of the AC-DE interface.

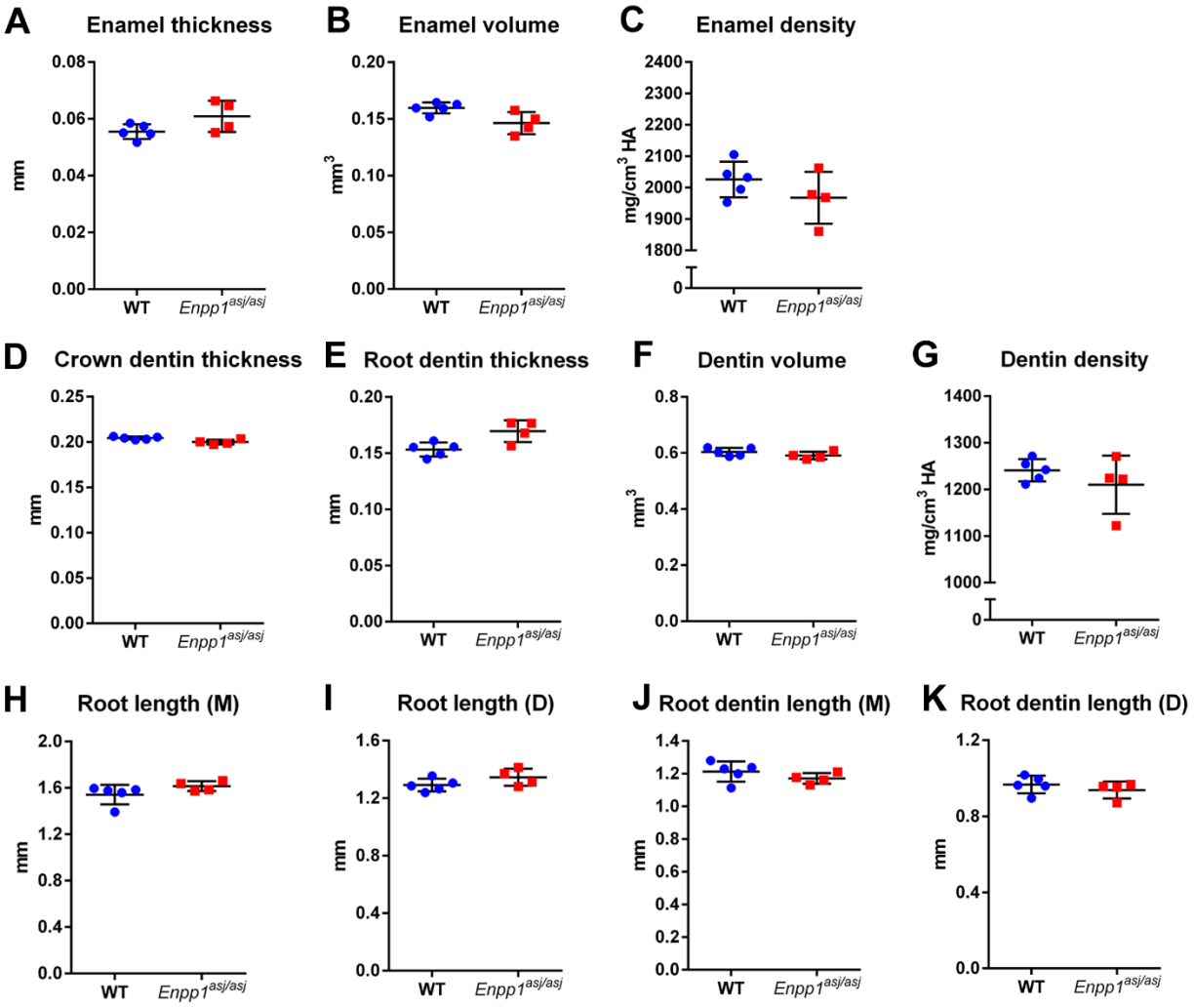

Appendix Figure 12. Microcomputed tomography analysis of dental tissues in *Enpp1* mutant mice. Wild-type (WT) and *Enpp1*$^{asj/asj}$ mouse first mandibular molars at 12 weeks were scanned by high resolution micro-CT. All linear, volumetric, and density measurements in enamel and dentin exhibited no significant differences (adjusted p>0.05) for *Enpp1*$^{asj/asj}$ vs. WT mice.

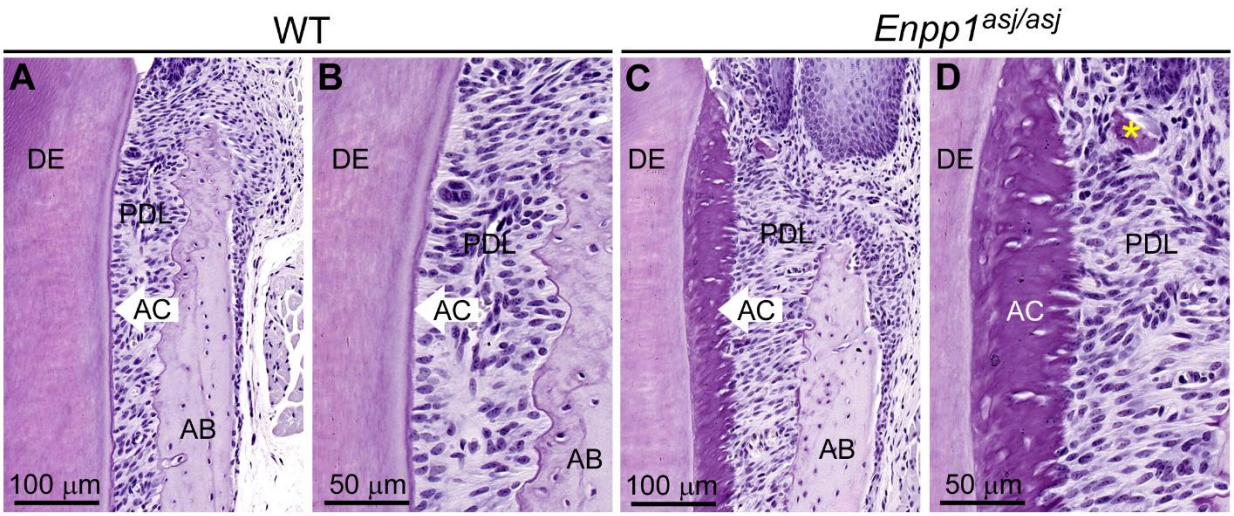

Appendix Figure 13. Histology of dental tissues in *Enpp1* mutant mice. Histology sections of **(A, B)** wild-type (WT) first mandibular molars compared to **(C, D)** *Enpp1*$^{asj/asj}$ molars at 12 weeks reveal dramatically increased acellular cementum (AC) in *Enpp1*$^{asj/asj}$ mice. *Enpp1*$^{asj/asj}$ molars exhibit embedded nucleated cementocyte-like cells and empty lacunae (D) unusual for cervical cementum. *Enpp1*$^{asj/asj}$ mice exhibit cementicles (yellow star in D) in the periodontal ligament (PDL) space on buccal aspects of molars, also evident by micro-CT analysis shown in Figure 5. DE= dentin; AB = alveolar bone.

Appendix Table 1. Summary of teeth analyzed from GACI subjects and age-matched healthy controls.

Subject	Gender	Tooth type	Tooth number	Age at tooth loss (years)	Extraction/ exfoliation
Control 1	F	Lateral incisor	D	7	Exfoliation
Control 2	M	Central incisor	E	9	Extraction
		Central incisor	F	9	Extraction
Control 3	F	Central incisor	E	8	Exfoliation
		Lateral incisor	D	8	Exfoliation
Control 4	F	Canine	C	~11	Exfoliation
GACI subject 1	F	Canine	C	7	Extraction
		Lateral incisor	D	7	Extraction
		Lateral incisor	G	7	Extraction
		Canine	H	7	Extraction
GACI subject 2	F	Lateral incisor	D	8	Extraction
		Central incisor	E	8	Extraction
		Central incisor	F	8	Extraction
		Lateral incisor	G	8	Extraction
GACI subject 3	M	Lateral incisor	N	6	Extraction
		Lateral incisor	Q	6	Extraction
GACI subject 4	F	N/A	N/A	N/A	N/A
GACI subject 5	M	N/A	N/A	N/A	N/A

Appendix Table 2. Biochemical results for GACI subjects.

Test	Normal range	Subject 1 (6.5 yrs)	Subject 2 (7.11 yrs)	Subject 3 (6.11 yrs)	Subject 4 (26.5 yrs)	Subject 5 (25.7 yrs)
Calcium	2.15-2.55 mmol/L	2.35	2.42	2.45	2.32	2.33
Phosphorus (Inorganic)	3.0-5.7 mg/dL	3.2	**2.8**	3.0	**2.3**	**1.9**
Phosphorus (Inorganic; Urine)	7-148 mg/dL	**366**	11	102	71	53
Alkaline phosphatase (ALP)	69-325 U/L	**349**	173	278	96	121
Inorganic pyrophosphate (PP_i)	11.9 ± 2.0[A] μM	**0**	N/A	**2.4**	N/A	**0.2**
25-Hydroxyvitamin D (25-OH, D; Total)	20-40 ng/mL (pediatric) 20-79 ng/mL (adult)	**18**	**19**	37	45	**19**
Parathyroid hormone (PTH; intact)	15.0-65.0 pg/L	62.6	**85.9**	42.4	**67.9**	30.6
Intact fibroblast growth factor 23 (iFGF23)	22.2-63.6 pg/ml	**116**	29	**89**	**128**	**78**[B]
C-terminal (cFGF23)	≤ 230 RU/ml (pediatric) ≤ 180 RU/ml (adult)	**447**	104	206	180	124[B]

The ages in years (yrs) denote the time point of lab testing performed for respective subjects. Bold font indicates values outside of the normal range.

N/A = Not available. RU = Reference units.

[A] There is no established normal range for PP_i concentrations. We report here the mean ± SD in units of μM for n=3 unaffected control individuals.

[B] Subject 5 posted FGF23 findings of 226 pg/ml iFGF23 and 339 RU/ml cFGF23 when measured 3.5 yrs earlier, though FGF23 levels have normalized since that time.

Appendix Table 3. Micro-computed tomography measurements of exfoliated/extracted teeth from GACI subjects and age-matched healthy controls.

Subject	**Gender**	**Tooth**	**Cementum thickness** (μm)	**Cementum density** (mg/cm^3 HA)	**Enamel density** (mg/cm^3 HA)	**Dentin density** (mg/cm^3 HA)
Control 1	F	Lateral incisor (D)	55	822.40	2097.05	1194.68
Control 2	M	Central incisor (E)	75	893.83	2144.53	1100.10
		Central incisor (F)	78	958.09	2194.83	1123.21
Control 3	F	Central incisor (E)	93	783.55	2105.46	1114.77
		Lateral incisor (D)	65	792.54	2182.63	1188.01
Control 4	F	Canine (C)	48	813.86	2024.39	1075.03
GACI subject 1	F	Canine (C)	333	1035.05	2182.94	1125.56
		Lateral incisor (D)	212	1093.04	2177.49	1180.83
		Lateral incisor (G)	194	1083.81	2200.87	1164.06
		Canine (H)	325	1040.44	2247.73	1169.61
GACI subject 2	F	Lateral incisor (D)	227	1051.97	2207.08	1187.05
		Central incisor (E)	299	949.76	2026.81	1091.95
		Central incisor (F)	288	1032.43	2127.20	1147.11
		Lateral incisor (G)	264	1051.24	2184.14	1168.48
GACI subject 3	M	Incisor 1 (N)	281	967.01	2086.34	1079.28
		Incisor 2 (Q)	327	1036.71	2113.74	1105.88